AGU PUBLICATIONS

JGR

Journal of Geophysical Research: Oceans

RESEARCH ARTICLE

10.1002/2016JC011655

A numerical model for the entire Wadden Sea: Skill assessment and analysis of hydrodynamics

Ulf Gräwe[1], Götz Flöser[2], Theo Gerkema[3], Matias Duran-Matute[3,4], Thomas H. Badewien[5], Elisabeth Schulz[6], and Hans Burchard[1]

[1]Department of Physical Oceanography and Instrumentation, Rostock, Leibniz Institute for Baltic Sea Research Warnemünde, Germany, [2]Helmholtz-Zentrum Geesthacht, Institute for Coastal Research, Geesthacht, Germany, [3]Department of Estuarine and Delta Systems, Royal Netherlands Institute for Sea Research, Den Burg, Netherlands, [4]Department of Applied Physics, Eindhoven University of Technology, Eindhoven, Netherlands, [5]Carl-von-Ossietzky University, Institute for Chemistry and Biology of the Marine Environment, Wilhelmshaven, Germany, [6]IFREMER, Laboratoire de Physique Hydrodynamique et Sédimentaire, Plouzané, France

Key Points:
- This is the first 3-D hydrodynamic model of the entire Wadden Sea
- The model results compare well to various types of observations
- Different estimates for exchange flow have been made

Correspondence to:
H. Burchard,
hans.burchard@io-warnemuende.de

Citation:
Gräwe, U., G. Flöser, T. Gerkema, M. Duran-Matute, T. H. Badewien, E. Schulz, and H. Burchard (2016), A numerical model for the entire Wadden Sea: Skill assessment and analysis of hydrodynamics, *J. Geophys. Res. Oceans*, *121*, 5231–5251, doi:10.1002/2016JC011655.

Received 17 JAN 2016
Accepted 9 JUN 2016
Accepted article online 16 JUN 2016
Published online 31 JUL 2016

Abstract A baroclinic three-dimensional numerical model for the entire Wadden Sea of the German Bight in the southern North Sea is first assessed by comparison to field data for surface elevation, current velocity, temperature, and salinity at selected stations and then used to calculate fluxes of volume and salt inside the Wadden Sea and the exchange between the Wadden Sea and the adjacent North Sea through the major tidal inlets. The model is simulating the reference years 2009–2011. An overview of tidal prisms and residual volume fluxes of the main inlets and their variability is given. In addition, data from an intensive observational campaign in a tidal channel south of the island of Spiekeroog as well as satellite images and observations of sea surface properties from a ship of opportunity are used for the skill assessment. Finally, the intensity of estuarine overturning circulation and its variability in the tidal gullies are quantified and analyzed as function of gravitational and wind straining using various estimates including Total Exchange Flow (TEF). Regional differences between the gullies are assessed and drivers of the estuarine circulation are identified. For some inlets, the longitudinal buoyancy gradient dominates the exchange flow, for some others wind straining is more important. Also the intensity of tidal straining (scaled covariance of eddy viscosity and vertical shear) depends on buoyancy gradient and wind forcing in different ways, depending on local topography, orientation toward the main wind direction, and influence by freshwater run off inside or outside the tidal basin.

1. Introduction

The Wadden Sea in the south-eastern North Sea extends from southern Denmark in the north to northern Holland (The Netherlands) in the southwest and is characterized by a chain of barrier islands, separated by tidal inlets leading into the back barrier basins, through tidal gullies with ebb-tidal deltas on the seaward end and branching tidal channels on the landward end leading to extensive intertidal flats (see Figure 1). This pattern is interrupted by three major tidal estuaries, the Ems, the Weser, and the Elbe, providing the German Bight with large amounts of fresh water [see *Reise et al.*, 2010 for a general description of the Wadden Sea].

In this part of the North Sea, the tide propagates along the coast of Holland and then along the Wadden Sea toward Denmark. The tidal range increases toward the German Bight (to more than 3 m) and then decreases again toward the North; tidal phases between the extreme ends of the Wadden Sea differ by about 8 h [*Postma*, 1982].

The exchange of water (along with nutrients and suspended matter) between the North Sea and the Wadden Sea, through the inlets, is primarily due to tides. The volume of water entering a basin during flood, and leaving it during ebb, is called the tidal prism. For the entire Wadden Sea, empirical values for the tidal prism were listed by *Postma* [1982], except for some inlets for which no data was available. The actual volumes entering and leaving on any particular day are however affected by the wind as well as the spring-neap cycle. A numerical modeling study for the Dutch Wadden Sea showed that this variability, calculated

© 2016. American Geophysical Union. All Rights Reserved.

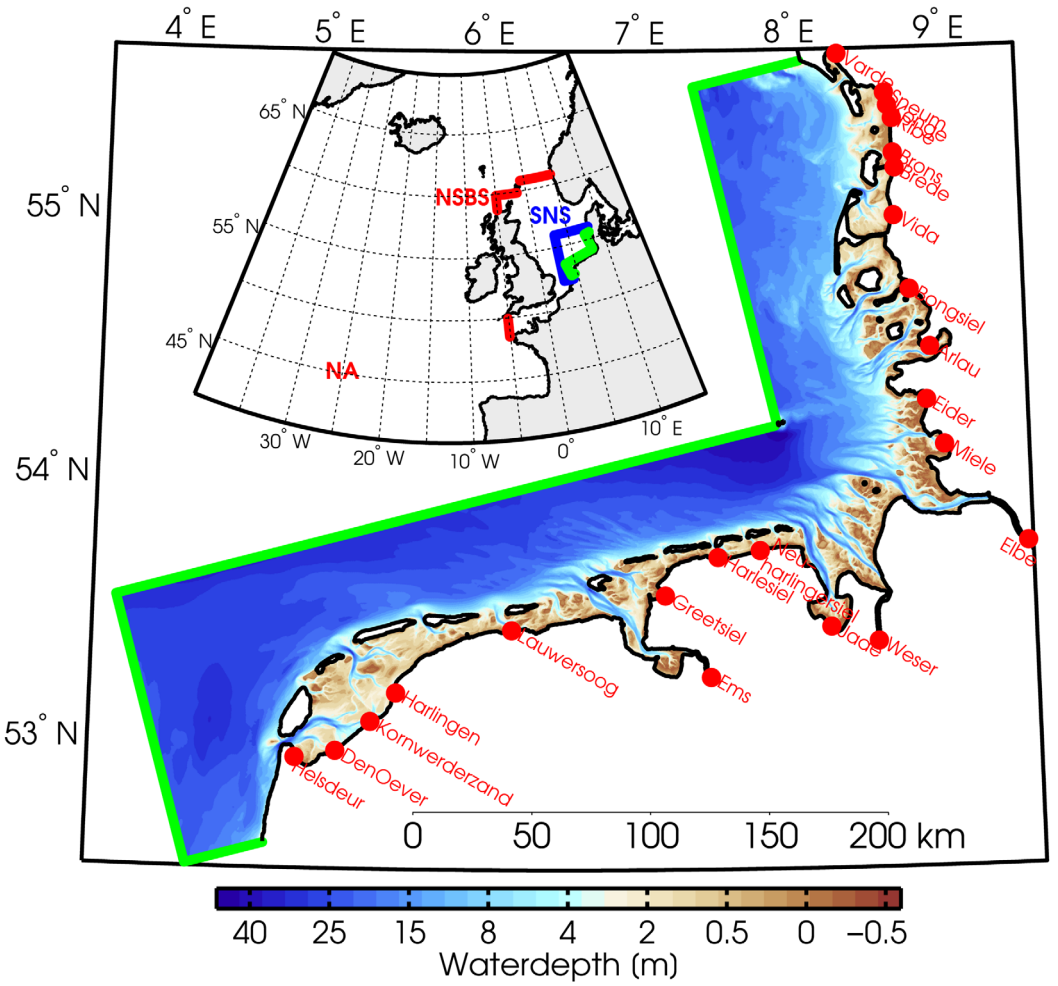

Figure 1. Large map: Wadden Sea model including bathymetry (color coded), coastline (black lines), and freshwater runoff locations (red dots). Small map upper left: Hierarchy of nested model domains: NA: North East Atlantic model (2-D), NSBS: North Sea—Baltic Sea model (3-D, boundaries shown in red), SNS: Southern North Sea (3-D, boundaries shown in blue), and the Wadden Sea model (3-D, boundary shown in green). The red dots and text denote the freshwater sources (see Table 1 for the runoff statistics).

as the standard deviation over a 2 year record, amounts to about 20% of the long-term mean tidal prism [*Duran-Matute et al*., 2014].

In the present study, we extend this to the entire Wadden Sea, providing estimates for all major inlets. We obtain these results from three-dimensional numerical simulations carried out with the General Estuarine Transport Model (GETM), at a horizontal resolution of 200 m and with terrain-following vertical coordinates with 26 layers. We concentrate on the years 2009–2011, for which we impose meteorological forcing, freshwater discharge, and boundary conditions for tidal forcing and storm surges. The simulation was spun up during the entire year 2008, of which the second half was used for calibrating parts of the bathymetry to obtain better results for the reproduction of tidal gauge data.

The present study attempts to numerically reproduce the baroclinic dynamics of the entire Wadden Sea with one single model setup at such a high-resolution, that all major tidal inlets are resolved with a few grid points at least. Previous baroclinic studies examined specific regions, such as *Duran-Matute et al*. [2014] for the Dutch Wadden Sea, *Staneva et al*. [2009] for the East Frisian Wadden Sea (i.e., the most westerly part of the German Wadden Sea, between the Ems and Jade estuaries), and *Purkiani et al*. [2015, 2016] for the Sylt-Rømø bight in the Northern Wadden Sea. All these baroclinic Wadden Sea studies used GETM.

Such a configuration for the entire Wadden Sea is necessary to quantify and explain the regional differences as well as the connectivity between the different parts of the Wadden Sea in a comparative way. While local

studies of specific Wadden Sea basins in high-resolution help to understand the processes within these basins and may help to explore general features of Wadden Sea basins and similar coastal systems, only a model for the entire Wadden Sea provides fluxes between basins and their relation to each other. The correct quantification of residual (i.e., tidally averaged) volume fluxes is necessary to explain fluxes of fine sediments and dissolved substances such as nutrients. Such volume fluxes and tidal prisms have for example been calculated by *Duran-Matute et al.* [2014] for the Dutch Wadden Sea (using a 3-D baroclinic configuration of GETM) and by *Herrling and Winter* [2015] for the East Frisian Wadden Sea using a 2-D configuration of Delft-3-D. However, absolute numbers of the interbasin exchange within both regions cannot be made due to various differences in model numerics, model mode (2-D or 3-D, baroclinic or barotropic), or model forcing (inclusion of storm surges or idealized boundary forcing).

Such a quantification of volume fluxes within the Wadden Sea is a basis for the estimation of sediment fluxes, which depend critically on volume fluxes itself [*Staneva et al*., 2009; *Lettmann et al*., 2009; *Nauw et al*., 2014; *Sassi et al*., 2015], but also on residual circulation [*Burchard et al*., 2008], (J. Becherer et al., Estuarine circulation vs tidal pumping: Sediment transport in an energetic tidal inlet, submitted to *Journal of Geophysics Research*, 2016). The latter may have several different drivers such as gravitational circulation, tidal straining circulation, and tidal pumping [*Burchard et al*., 2013], which may vary in their relevance between different tidal inlets. One of the goals of this study is to better understand the contributions from these different hydrodynamic drivers across different tidal inlets.

The transport of nutrients in the Wadden Sea is strongly linked to the sediment transport (due to the high organic matter content of the suspended matter) as well as to the water volume transport. Significant regional differences in the cycling of manganese and phosphorus have been observed and it has been hypothesized that hydrodynamic factors are among the drivers for these differences [*Kowalski et al*., 2012; *van Beusekom and de Jonge*, 2012]. Only a 3-D baroclinic hydrodynamic model for the entire Wadden Sea coupled to a suitable biogeochemical model could help to understand the mechanisms for this regional differentiation. Differences in hydrodynamics are often a key factor in the different morphodynamic evolution in the Wadden Sea basins [see, e.g., *Wang et al*., 2012; *Dissanayake et al*., 2012; *Herrling and Winter*, 2014].

Besides transport of suspended sediment and nutrients, also freshwater is transported through the Wadden Sea, originating from rivers and sluices, and leaving the Wadden Sea through the tidal inlets. Simultaneously, the salinity gradients themselves affect the circulation. Here we study the salt fluxes and their variability, validating the model results by comparisons with time series at several locations in the Wadden Sea. We also provide a list of key quantities like the tidal prisms and their variability.

This study is organized such that after this introduction (section 1) the numerical model GETM, the data sources and the analysis methods are briefly introduced (section 2), followed by a careful multiparameter model skill assessment (section 3). The estuarine circulation is then investigated in detail in section 4, using Eulerian exchange flow analysis (section 4.2) as well as Total Exchange Flow (TEF) [see *MacCready*, 2011] analysis (section 4.3). General conclusions are finally drawn in section 5.

2. Material and Methods

2.1. Numerical Model

The numerical model applied for the present study is the General Estuarine Transport Model (GETM) [*Burchard and Bolding*, 2002; *Hofmeister et al*., 2010] which has been specifically designed for coastal ocean simulations with substantial drying and flooding of intertidal flats. GETM is a three-dimensional baroclinic open source model with hydrostatic and Boussinesq assumptions. In GETM, the three-dimensional hydrostatic momentum equations are solved on a staggered C-grid, which is horizontally Cartesian in the present application. To calculate vertical turbulent fluxes, GETM uses turbulence closure models from the General Ocean Turbulence Model (GOTM) [*Umlauf and Burchard*, 2005], and in the present study a k-ε model is used with an algebraic second moment closure. For the vertical discretization, GETM uses bottom and surface following generalized vertical coordinates.

Higher-order positive-definite advection schemes are used for the advection of momentum, temperature, salinity, and turbulent quantities k (turbulent kinetic energy) and ε (dissipation of k into heat). High-

resolution coastal ocean simulations using GETM including drying and flooding of intertidal flats have for example been carried out before for the Dutch Wadden Sea [*Duran-Matute et al*., 2014; *Sassi et al*., 2015], the East Frisian Wadden Sea [*Stanev et al*., 2003; *Staneva et al*., 2009], the Sylt Rømø bight in the North Frisian Wadden Sea [*Burchard et al*., 2008; *Purkiani et al*., 2015, 2016], the Elbe estuary [*Burchard et al*., 2004], and Willapa Bay in Washington State [*Banas et al*., 2007].

2.2. Model Setup

The numerical model for the Wadden Sea is the end-member of a hierarchy of four nested models, see Figure 1. First, a vertically integrated North Atlantic model with a horizontal resolution of about 7.5 km forced with surface winds and air pressure (taken from the Climate Forecast System Reanalysis model) [*Saha et al*., 2010] was used to obtain surge levels at the open boundaries for the North Sea model (about 2 km horizontal resolution). The surge levels at the open boundaries were then superimposed to astronomic tidal elevations calculated by means of the Oregon State University Tidal Prediction Software (OSU-TPS). Furthermore, time varying profiles of salinity and temperature obtained from the Climate Forecast System Reanalysis (CFSR) meteorological data of the U.S. National Centers for Environmental Prediction (NCEP) were used for the three-dimensional boundary conditions of the North Sea model. For this North Sea setup, salinity, temperature, freshwater discharge, and complete meteorological forcing are all taken into account. Assessment and analysis of the North Sea model are described in *Gräwe et al*. [2015]. Next, a three-dimensional southern North Sea setup with a 600 m resolution and 42 vertical layers was used. The salinity and temperature data at a temporal resolution of 2 h were extracted for the boundary conditions, as well as surface elevations at a temporal resolution of 20 min.

Finally, the Wadden Sea model is the highest-resolution level of this model hierarchy. The Wadden Sea model bathymetry is based on data which have been provided by Dutch Rijkswaterstaat (resolution 20 m), the German project AufMod (resolution 50–200 m), and the Danish Maritime Safety Administration (resolution 200 m). Based on these data, a bathymetry for the entire Wadden Sea has been constructed, with a resolution of 200 m on a Cartesian grid which has been rotated in anticlockwise sense by 18° to better match the coastline (see Figure 1). With this, the grid consists of 1339 $\times$ 1865 grid points, with 780,000 actively calculated water points, resulting in a ratio of 32% active to total points. After the subdomain decomposition and the removal of empty subdomains, the wet point ratio increased to 89%. Lateral boundary conditions for surface elevation and depth-mean current velocity are extracted from the 600 m model every 20 min, and vertical profiles for temperature and salinity are extracted every hour. Those boundary values are linearly interpolated in time and space to the open boundary grid of the 200 m model.

For the 200 m Wadden Sea model, GETM uses a micro time step of 4 s for the external mode and a macro time step of 40 s for the internal mode (i.e., a splitting factor of 10). Twenty six adaptive coordinate layers [see *Hofmeister et al*., 2010] are used for the vertical discretization. To parameterize unresolved lateral eddy transport of salinity, the Smagorinsky formulation with an empirical parameter of 0.3 was used. The domain is subdivided into 800 subdomains, each of them being allocated to one core of the supercomputer at the North-German Supercomputing Alliance (HLRN). The setup shows an almost linear scaling over a wide range of subdomain sizes (varying from 25 $\times$ 25–35 $\times$ 35). For large subdomains, the cache size is the limiting factor. For smaller subdomains, the ratio of computational grid points to (parallel) exchange grid points becomes worse, such that the communication overhead increases. With this configuration, 18 h are required to simulate 1 year.

2.3. Meteorological and RunOff Forcing

The larger models (North Atlantic, North Sea) were forced by NCEP-CFSR meteorological data at a resolution of 1/3° and 1 h. Meteorological forcing for the Southern North Sea and the Wadden Sea model was obtained from the operational forecast model of the German Weather Service (DWD). The available variables are 10 m wind speed and direction, and 2 m dry air temperature and dew point temperature, as well as precipitation and cloudiness, which are discretized in a grid with a resolution of $1/16°$ ($\sim$7 km) and have a temporal resolution of 3 h. From these meteorological data, the surface momentum, heat, and freshwater fluxes are calculated using the bulk formulae by *Kondo* [1975]. As water type for the absorption of solar radiation the Jerlov-III type was applied, and as bottom roughness length a constant value of $z_0 = 10^{-3}$ m was used, being slightly lower than the value chosen by *Duran-Matute et al*. [2014] for a Western Dutch Wadden

Table 1. Freshwater Fluxes From Point Sources Into the Wadden Sea (See Map in Figure 1 for the Locations)[a]

Name	Mean	Max	Std
Varde	12.80	15.58	1.95
Sneum	3.68	4.63	0.77
Konge	7.67	10.27	1.54
Ribe	10.52	14.09	2.21
Brons	1.24	1.50	0.22
Brede	4.28	5.42	1.05
Vida	3.60	4.72	0.88
Bongsiel	7.66	52.13	6.96
Arlau	3.15	31.03	3.79
Eider	31.61	201.11	28.24
Miele	2.63	19.50	2.81
Elbe	765.75	3358.13	466.33
Weser	243.16	478.17	82.28
Jade	8.70	56.67	7.93
Harlesiel	2.63	19.50	2.81
Neuharlingersiel	3.15	31.03	3.79
Greetsiel	2.63	19.50	2.81
Ems	102.73	176.17	38.70
Lauwersoog	38.73	1254.82	93.29
Harlingen	5.03	68.02	8.57
Kornwerderzand	198.78	1661.02	316.11
Den Oever	231.10	2288.66	374.36
Helsdeur	8.59	105.32	1.57

[a]Given are the mean and the maximum (max) values and the standard deviation (std) in $m^3\ s^{-1}$ for the years 2009–2011.

Sea model. Although the model performance does not strongly depend on a variation of z_0 by a factor of two, this may explain some of the quantitative differences between the two models.

The model is further forced by freshwater runoff from point sources at the coastline, see Table 1 and Figure 1. The Dutch runoff data are provided by the Royal Netherlands Institute for Sea Research and Rijkswaterstaat (temporal resolution is 15 min), the data for the East Frisian Wadden Sea are from the German Bundesamt für Gewässerkunde (daily resolution), and those for the North Frisian and the Danish Wadden Sea are from Schleswig-Holstein's Government-Owned Company for Coastal Protection, National Parks, and Ocean Protection (daily). Data for the larger rivers are from the UK's Centre for Environment, Fisheries, and Aquaculture Science (daily).

To get an impression of the complex forcing situation, a few forcing data are shown in Figure 2 for the year 2010. The wind forcing (taken from the station Spiekeroog) shows typical wind speeds of 5–10 m s^{-1} in autumn and winter, with peak wind speeds reaching 15 m s^{-1} and significantly lower wind velocities of typically below 5 m s^{-1} during spring and summer. The most common wind

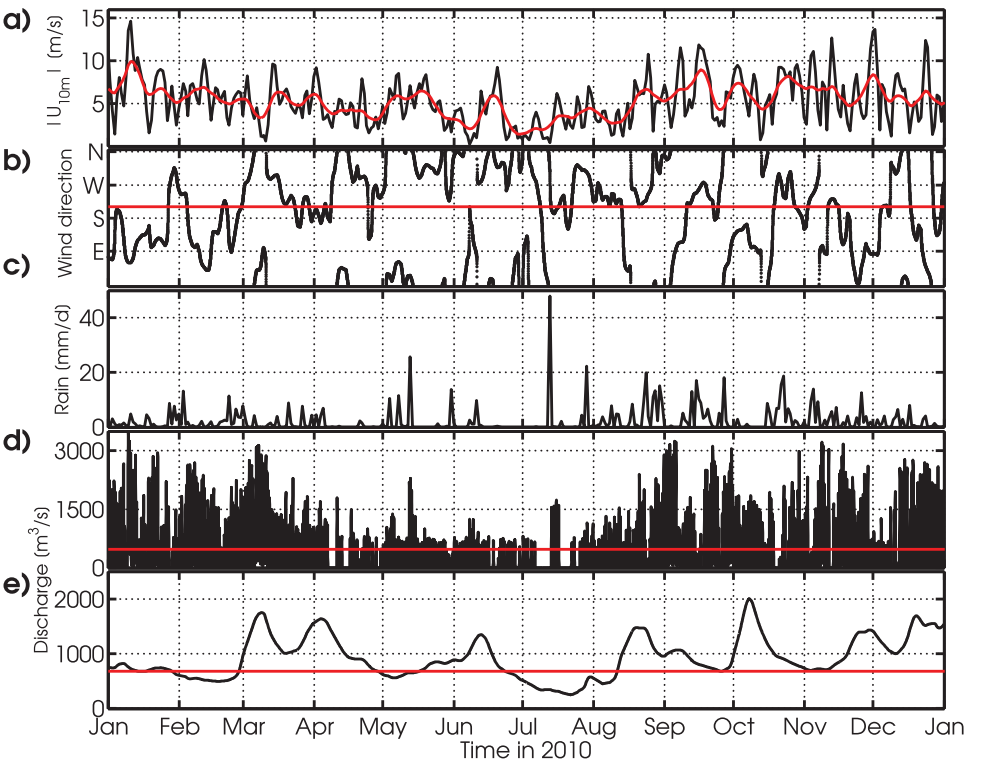

Figure 2. Time series of (a) daily averaged wind speed at Spiekeroog. The red line indicates the time series smoothed with a 7 day running mean. (b) Daily averaged wind direction. The red line marks the mean wind direction. (c) Daily averaged precipitation in l/day. (d) Hourly freshwater discharge of the Lake IJssel. (e) Hourly freshwater discharge of the Elbe.

Table 2. Complex Correlation Coefficients of the Zonal and Meridional Component of the 10 m Wind Speed for the Period 2009–2011[a]

Station	Marsdiep	Spiekeroog	Sylt
Marsdiep	1	0.89 + 0.21i	0.78 + 0.17i
Spiekeroog		1	0.92 + 0.09i
Sylt			1

[a]The real part gives the correlation coefficient for the eastward (*u*) component and the imaginary part gives the correlation coefficient for the northward (*v*) component. The wind data are taken from the atmospheric model of the DWD.

direction is south-westerly, but some storm events (such as in January 2010) may also occur at easterly wind directions. The zonal wind component is highly correlated over the entire Wadden Sea, as indicated by the real parts of the complex correlation between the stations Spiekeroog, Sylt, and Marsdiep show (see Table 2).

Precipitation is highly intermittent (see Figure 2c), with more rain during autumn than winter, but single peak events with rates exceeding 40 mm d^{-1} may occur during summer.

The Dutch part of the Wadden Sea is strongly influenced by the highly regulated discharge from Lake IJssel (Figure 2d), due to the operation of sluices at Kornwerderzand and Den Oever (see Figure 1 for the locations). Following the seasonality of precipitation, discharges from Lake IJssel are smallest during spring and summer. During autumn and winter, peak discharge values of > 3000 m^3 s^{-1} can be reached. Discharge from River Elbe (Figure 2e) peaks during late winter (high precipitation) and early spring (snow melt) and early autumn (high precipitation) with maximum values of 2000 m^3 s^{-1} and mean values of 800 m^3 s^{-1}.

3. Model Skill Assessment

3.1. Tidal Propagation

In the model, all major tidal constituents are implicitly included via the boundary conditions for surface elevation. The main tidal constituent in the North Sea is the semidiurnal lunar M_2 which propagates in an anticlockwise sense as a Kelvin-type wave through the North Sea. The observed phase difference of the M_2 tide between Den Helder at the south-west edge of the Wadden Sea and Esbjerg at its north-east edge is about 215° (7.4 h, in agreement with the estimate by *Postma* [1982]), see Table 3. In the model simulation, the M_2 tide is reproduced with typical errors of 5% for the amplitude and 10 min for the phase. Largest errors occur at sheltered inland locations where the approach channels may not have been sufficiently resolved (see, e.g., the gauge at Spiekeroog).

Since the nonlinear overtides are also relevant for tidal pumping of solutes and particulate matter [*Gräwe et al.*, 2014], the M_4 tide is examined here in further detail for the same gauge stations. Table 3 shows again

Table 3. Summary of Error Measures for the Model Skill Assessments of the SSH (2009–2010)[a]

	Astronomical				Residual
	M_2		M_4		
Station	Amplitude (m)	Phase (°)	Amplitude (m)	Phase (°)	RMSE (m)
Cuxhaven	1.38,1.45 (**5**%)	10, 9 (−2 min)	0.12,0.11 (1%)	266,248 (−**18** min)	0.07
Dagebüll	1.30,1.24 (−**4**%)	45, 41 (−**8** min)	0.14,0.14 (−2%)	305,318 (**13** min)	0.08
Delfzijl	1.35,1.20 (−**12**%)	332,340 (**16** min)	0.19,0.17 (−10%)	134,167 (**33** min)	0.08
Den Helder	0.65,0.69 (**7**%)	190,191 (2 min)	0.11,0.14 (**25**%)	219,231 (**12** min)	0.07
Eidersperrwerk	1.36,1.37 (0%)	19, 14 (−**10** min)	0.15,0.14 (−7%)	264,249 (−**15** min)	0.11
Esbjerg	0.68,0.62 (−10%)	35,45 (**22** min)	0.06,0.05 (−13%)	237,231 (−6 min)	0.11
Harlingen	0.84,0.85 (1%)	276,274 (−4 min)	0.11,0.10 (−9%)	88, 65 (−**23**min)	0.07
Helgoland	0.98,1.03 (5%)	310,322 (**24** min)	0.06,0.06 (2%)	143,172 (**29** min)	0.09
Huibertgat	1.03,0.88 (−14%)	277,282 (**10** min)	0.09,0.08 (−6%)	27, 33 (6 min)	0.07
Lauwersoog	1.04,0.89 (−**15**%)	286,286 (0 min)	0.12,0.11 (−10%)	40, 35 (−5 min)	0.07
List/Sylt	0.82,0.84 (**3**%)	52, 39 (−**26** min)	0.06,0.06 (−3%)	272,259 (−**13** min)	0.08
Nes	0.95,0.82 (−**14**%)	279,282 (**6** min)	0.10,0.07 (−**23**%)	15, 58 (**43** min)	0.07
Norderney	1.13,1.03 (−**9**%)	315,317 (**4** min)	0.03,0.03 (9%)	103,117 (14 min)	0.08
Pellworm	1.44,1.42 (−1%)	19, 15 (−**8** min)	0.13,0.12 (−7%)	225,217 (−8 min)	0.08
Spiekeroog	1.23,1.18 (−**4**%)	332,330 (−**4** min)	0.02,0.04 (**107**%)	162,173 (11 min)	0.11
Vlielandhaven	0.80,0.78 (−**3**%)	237,232 (−**10** min)	0.04,0.05 (**23**%)	309,295 (−**14** min)	0.07
Wilhelmshaven	1.74,1.67 (−**4**%)	0, 7 (**15** min)	0.10,0.09 (−11%)	170,152 (−**18** min)	0.07

[a]In the left columns, the comparison with the M_2 and M_4 is given. The first value gives the observation, the second one the simulated one. In parenthesis, we give the deviation in percent for the amplitude and in minutes for the phase. Bold values indicate statistically significant deviations. In the last column, the RMSE for the residual SSH is presented.

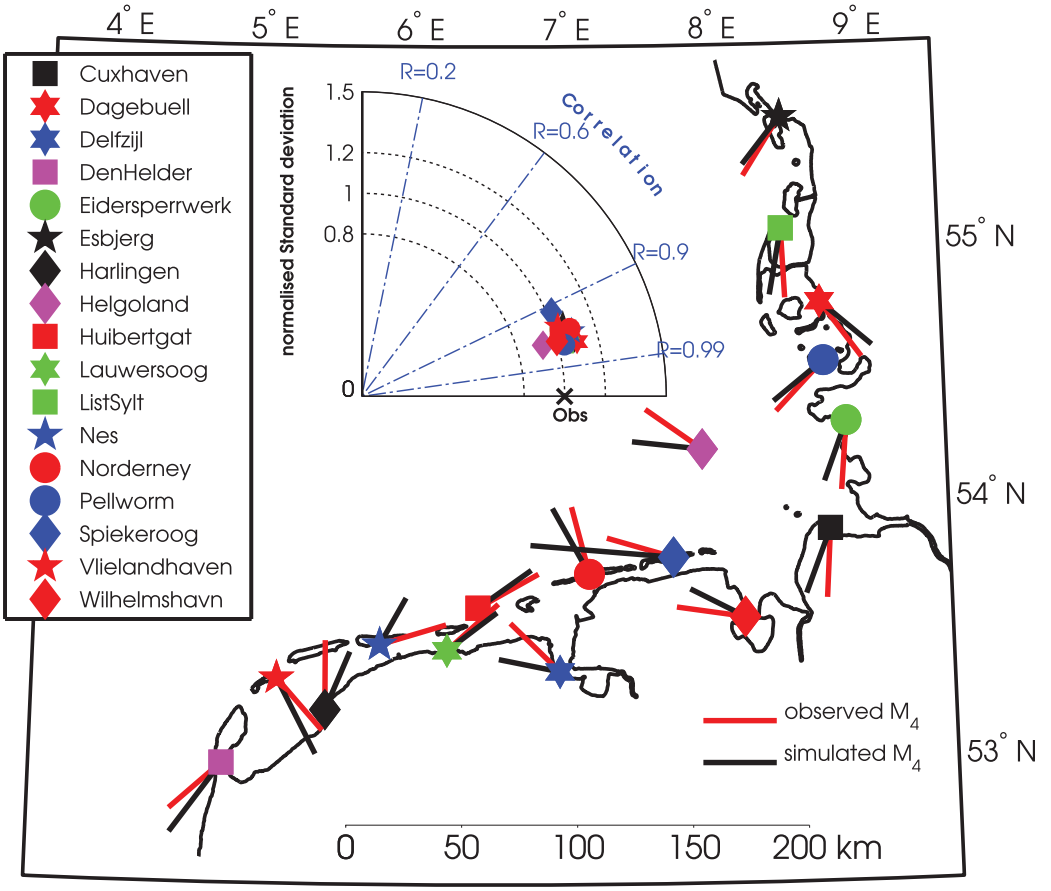

Figure 3. Comparison between the simulated and observed characteristics of the M_4 tidal constituent at selected tidal gauges. The length of the arrow represents the normalized amplitude of the M_4 tidal constituent. The observations (red arrow) have a length of unity. The angle of the arrow represents its phase lag in degrees. The insert shows the Taylor diagram for the model skill assessment of the surge elevations.

amplitude and phase errors. Typical errors for the M_4 tide are a few centimeters and phase errors are typically less than 15 min. It should be noted that the M_4 tide is difficult to reproduce, since it is strongly influenced by local bathymetry which is in parts still poorly resolved. The quality of the reproduction of the M_4 tide is also graphically displayed in Figure 3 as clock hand diagrams for all tidal gauges.

Finally the detided surge levels are validated in Table 3 (last column). Typical deviations between observations and model simulations is less than 10 cm. In addition, the Taylor diagram in Figure 3 shows the normalized standard deviation and the correlation between observations and model simulations for all stations for the period 2009–2011.

3.2. Temperature and Salinity Time Series

Since temperature and salinity determine the density of sea water which in turn has a substantial impact on the residual currents in the Wadden Sea, comparison of model results with these hydrographic properties is essential.

In *Duran-Matute et al.* [2014], a comparison was made between salinity measurements at the NIOZ-jetty (time series at 30 min sampling) and a similar model setup for the Dutch Wadden Sea. The agreement was good ($R^2 = 0.78$), capturing both seasonal and semidiurnal variations. For the model skill assessment of temperature and salinity time series, we consider here data from time series stations at the Jade, Hörnum (Sylt), Spiekeroog, Marsdiep, and the Lister Deep (between the islands of Sylt and Rømø), see Figure 4. The assessment was carried out in two different ways.

First, hourly values were used for the temperature and salinity analysis. This shows for temperature very high correlations of >0.99, due to the dominance of the annual cycle.

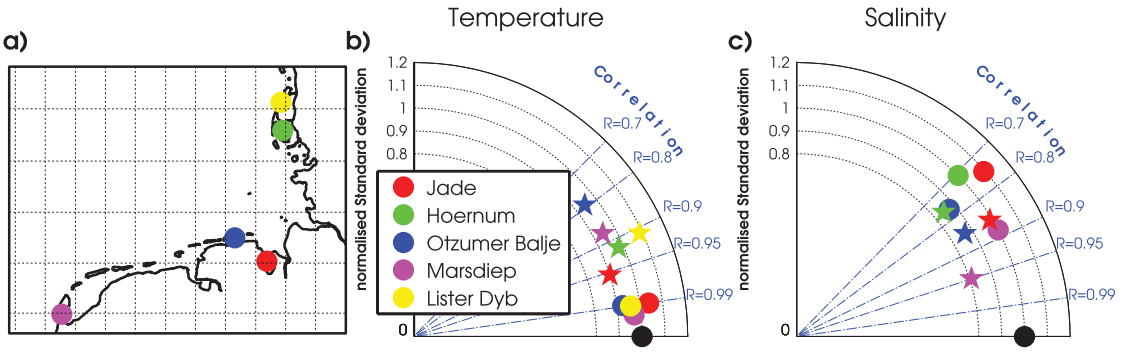

Figure 4. (a) Map of the Wadden Sea showing the location of the T/S assessment stations. (b) Taylor diagram for the assessment of the temperature. The full circles indicate the comparison with hourly values. The full stars show the model performance with the seasonal cycle removed. (c) Taylor diagram for the assessment of the salinity. The full circles indicate the comparison with hourly values. The full stars show the model performance after applying a 25 h running mean to remove the M_2 tidal signal.

To remove the annual cycle, we fitted a sinus with a period of 365 days to each observational data time series. Afterward, the fitted annual cycle was subtracted from the observed and simulated time series. After this removal of the annual cycle, the correlation for observed and simulated temperature are still high, with values around 0.9, and normalized standard deviations between 0.9 and 1.1. As expected, the correlation between simulated and observed salinity is worse, with correlation coefficients for hourly data ranging between 0.7 (Hörnum) and 0.9 (Marsdiep). The reason for the generally worse correlation for salinity as compared to temperature results from the fact that sea surface temperature (SST) is strongly triggered by surface heat fluxes (which in turn have been calculated by meteorological models using SST data assimilation). In contrast, salinity depends little on surface freshwater fluxes (precipitation, see Figure 2c), and mainly on remote riverine freshwater sources. For the Hörnum Deep, it is known that there is only little direct freshwater forcing, such that processes such as evaporation and laterally advective salinity transports dominate [see *Onken and Riethmüller*, 2010]. The removal of the annual cycle from the salinity observations has only a small effect on the assessment quality, since the annual cycle is typically not strongly developed [*Burchard and Badewien*, 2015].

As shown by several studies [*Becherer et al*., 2011; *Purkiani et al*., 2015; *Becherer et al*., 2015], horizontal density gradients may drive estuarine circulation in the Wadden Sea. A suitable model skill assessment for such density gradient data is provided by a ship of opportunity with a regular daily summer service between Büsum and the island of Helgoland. This ship is equipped with a FerryBox system operated by the Helmholtz-Zentrum Geesthacht as part of the COSYNA coastal observatory (http://www.hzg.de/institutes_platforms/cosyna/). Additionally, to close the gaps during the winter seasons, high-resolution analysis SST data from the OSTIA satellite programme (http://ghrsst-pp.metoffice.com/pages/latest_analysis/ostia.html) are used for model skill assessment here.

Figure 5 shows for the years 2009–2011 the comparison between SST anomaly from OSTIA, FerryBox, and GETM results and additionally between sea surface salinity anomaly (SSS) and sea surface density anomaly (SSD) from FerryBox and GETM. It can be seen how the temperature gradient alternates between winter and summer season, with warmer water near the coast during spring and summer and vice versa during autumn and winter. The salinity gradient is almost always directed offshore (saltier water in the North Sea), such that density gradients are generally directed offshore, as already shown by *Burchard et al*. [2008] from pole observations. A clear seasonality in the SSD cannot be seen, but typically stronger density gradients occur in spring (2009, 2010) or winter (2011). The general agreement between model results and observation is good. Specifically, the peak gradients in salinity and density in spring 2009 and 2010 and periods of weak gradients during summer are reproduced.

3.3. Currents

Surface currents (note that currents are generally positive, when directed landward) in the German Bight are continuously monitored by means of high-frequency (HF) radar systems installed near Büsum and on the islands of Sylt and Wangerooge. The obtained surface currents have a resolution of 1.5 km in space and 20 min. in time. These data have been recently used by *Stanev et al*. [2015] to obtain model and

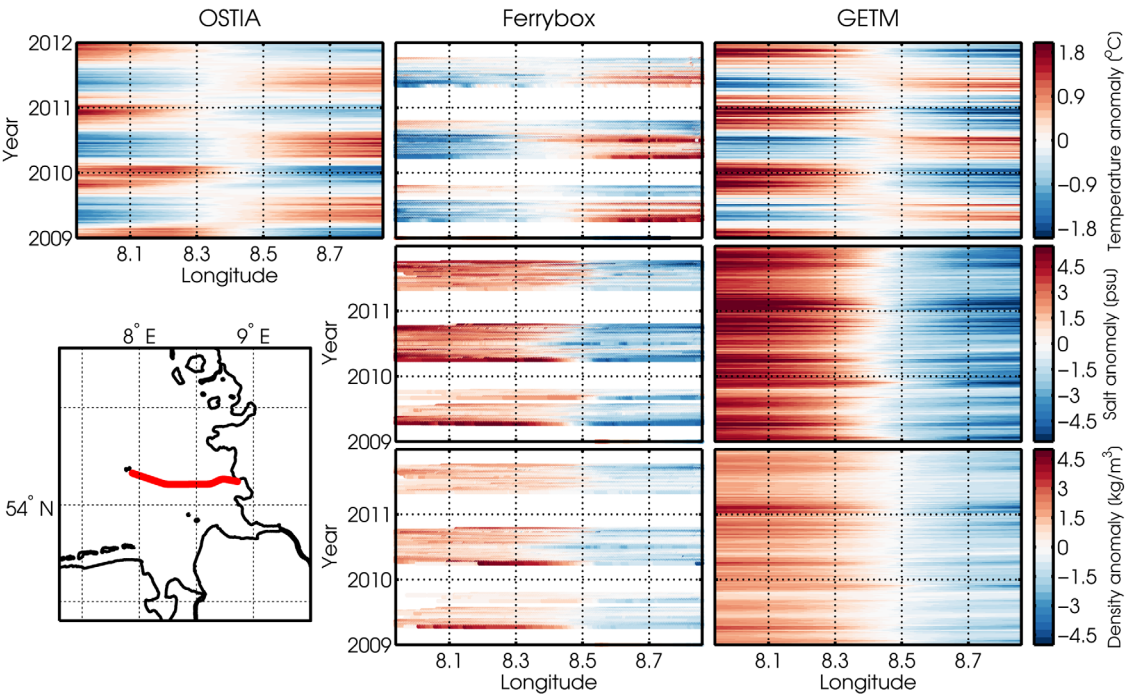

Figure 5. Comparison between sea surface temperature data (SST, top plots), sea surface salinity (SSS, middle plots), and sea surface density (SSD, bottom plots) from OSTIA (only SST) and FerryBox and GETM model simulations along a transect between Büsum and Helgoland (see inserted map) during the years 2009–2011. The white areas in the FerryBox observations indicate data gaps during the winter season. The following biases (root mean square errors) between the different data sets have been calculated: temperature FerryBox—GETM: 0.15 K (0.64 K); temperature FerryBox—Ostia: −0.14K (0.71 K); temperature GETM—Ostia: −0.3 K (0.43 K); salinity FerryBox—GETM: 0.43 psu (1.15 psu); density FerryBox—GETM: −0.17 kg m−3 (1.32 kg m−3).

observation-based state estimates for the surface currents in the German Bight, using the same numerical model (GETM) as in the present study.

Figure 6 shows a comparison between detided surface currents from observations and model simulations along a straight transect from Helgoland eastward toward the coast. It can be seen that the current is mostly directed northward, mainly due to the typically cyclonic circulation in the German Bight [see, e.g., *Staneva et al.*, 2009]. Strong south-westerly wind peaks cause strong residual currents in north-eastern direction along the entire transect (e.g., around 10 November and 4 December). North-easterly storms do also show some surface current signature with current toward the south-west (e.g., around 20 November and 12 December). Maximum residual surface currents in north-south direction amount to about 0.2 m s^{-1}. At times, currents localized near the west coast of Schleswig-Holstein are visible (e.g., the eastward-directed currents occurring around 20 November and 15 December). All features discussed above agree quite well between the observations and the model results, such that some confidence in the surface current simulations is given.

3.4. Transports

For two tidal inlets, data for tidally resolving volume fluxes observed by frequently crossing vessels equipped with Acoustic Doppler Currents Profilers (ADCPs) are available during the simulation period. These inlets are the Marsdiep (see inlet # 1 in Figure 7) and the Otzumer Balje (see inlet # 12 in Figure 7).

In the Marsdiep, the ferry boat between Den Helder on the mainland and the island of Texel crosses every half hour between 6 A.M. and 10 P.M. With the aid of various corrections and extrapolations, a value for the instantaneous through flux through the inlet is estimated [see *Buijsman and Ridderinkhof*, 2007 and *Nauw et al.*, 2014 for details]. The results for the data-model comparison during about 2 weeks show tidal volume flux amplitudes between $3 \cdot 10^4$ and $6 \cdot 10^4$ m^3 s^{-1}, depending on the phase of the spring-neap cycle (see Figure 8a). Shown are also results for the volume fluxes obtained by *Duran-Matute et al.* [2014] with their local model for the western Dutch Wadden Sea which is based on GETM with similar boundary conditions and a horizontal resolution of 200 m as well. The agreement between both model simulations and the data is excellent.

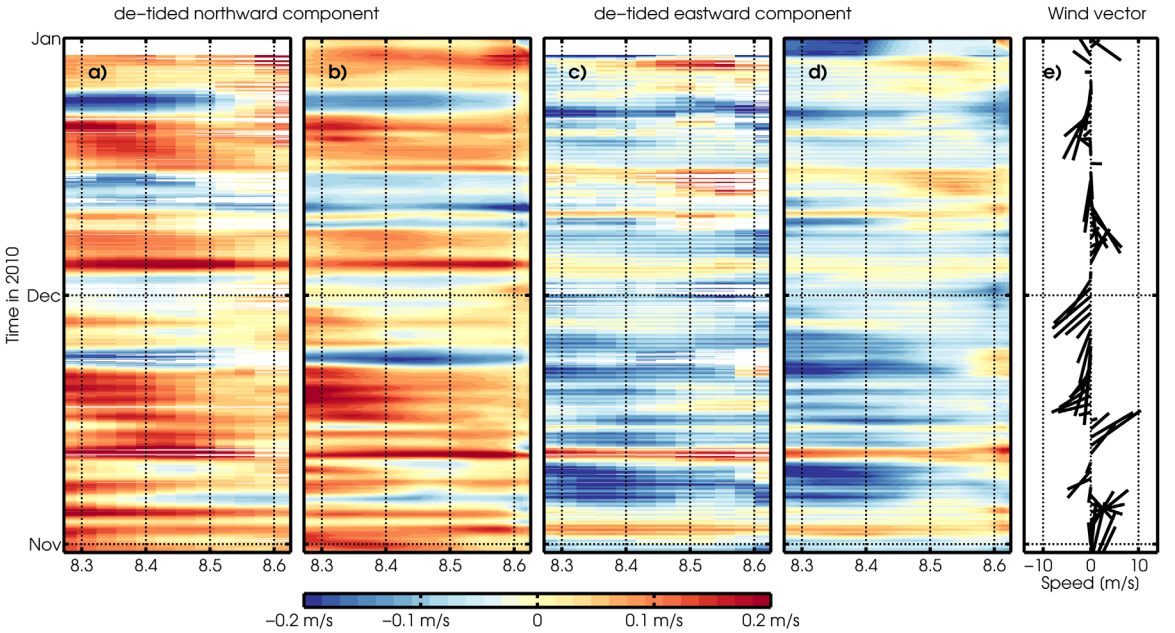

Figure 6. Comparison between model results and detided surface currents observed from HF radar along a straight transect extending eastward from the island of Helgoland during the months of November and December 201. (a) Detided northward component of surface current from observations; (b) detided northward component of surface current from model simulations; (c) detided eastward component of surface current from observations; (d) detided eastward component of surface current from model simulations; (e) stick plot of the daily averaged wind vector taken from the atmospheric model forcing data set (DWD).

Figure 8 shows the instantaneous flows, during a period of about a week, but it is also of interest to know what the net effect is, i.e., integrated over time, over a year for example. Since the net transport is much smaller than the gross transports during ebb or flood, errors (both in measurements and models) become relatively more important. It was demonstrated by *Sassi et al*. [2016] that gaps in space and time in the ADCP ferry measurements make the calculation of the annual mean transport unreliable. Besides, the model results show a huge variability, even in sign, of the annual-mean transport through the Marsdiep [*Duran-Matute and Gerkema*, 2015], as it depends strongly on the interannual variability of the wind statistics. As a result, it is not really meaningful to speak of "the" annual-mean transport as such.

At Otzumer Balje, ADCP transect data were obtained by scientists from ICBM (Institute for Chemistry and Biology of the Marine Environment, Wilhelmshaven, Germany) during a field campaign in May 2011 on board the research boat Otzum. The measurements were conducted in the Otzumer Balje, the tidal inlet between the islands of Langeoog and Spiekeroog. From 11 to 12 May, 130 transects were measured within 36 h. From 17 to19 May, more than 200 transects were measured within approximately 48 h. A downward-looking four beam broadband Acoustic Doppler Current Profiler (ADCP, RDI-Teledyne Workhorse sentinel, 1200 kHz) was used. The vertical resolution of the measured data is 0.25 m and the temporal resolution is 0.4 Hz. A Trimble SPS461 modular GPS Heading Receiver with OmniSTAR correction was used for positioning. The dual-antenna system records the heading of the vessel. During the field campaigns, current velocities reached maximum values of up to 1.6 m s^{-1}. The volume flux calculated from the current measurements amounts to around 12,000 m^3 s^{-1} during flood tide and 11,500 m^3 s^{-1} during ebb tide.

Figure 9 shows a comparison between the current speed observations and model simulations for two instants of time during the campaign. It is clearly visible that the numerical resolution of 200 m does not resolve details of the channel bathymetry such as the narrow deep part or the steep slope on the western side. On the other hand, the observations do not cover the entire transect due to small depth on the western side. Nonetheless, the current speed and its lateral distribution are quantitatively reproduced.

The observed volume flux amplitude in the Otzumer Balje is about 10^4 m^3 s^{-1}, including some temporal variability, which is reproduced by the model simulations (see Figure. 8b). During slack tide after each flood, a little kink is visible in the data, which probably results from hypsometric effects and this kink is not visible in the simulation data. This could be explained by the strong overestimation of the simulated M_4 tidal amplitude at the Spiekeroog tidal gauge (see Figure 3), resulting from relatively coarse resolution of this small tidal basin.

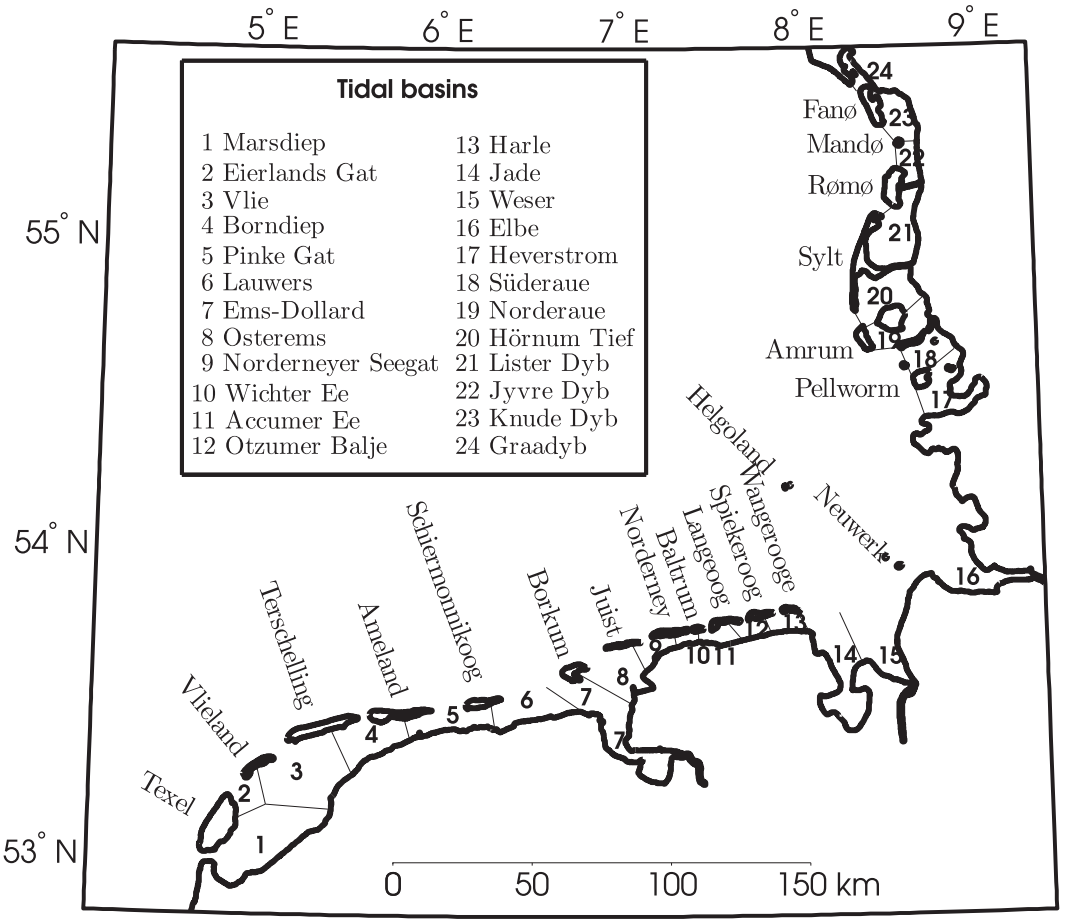

Figure 7. Map of the German Bight with geographical names of island and inlets.

4. Estuarine Circulation

4.1. Volume Fluxes

The long-term residual transports of water reflect one major transport mechanism for solutes in the Wadden Sea, whereas suspended particulate matter (SPM) transport may at times strongly deviate from the mean water transports. Tidal exchanges of water through inlets or across watersheds can be characterized by two quantities: the tidal prism (average time-integrated volume flux during ebb or flood through tidal inlets and across watersheds, in m^3) and the long-term residual flow, in $m^3\ s^{-1}$. It has already been shown in section 3.4 that the residual fluxes are characterized by a strong temporal variability. Still, the long-term averages are of general interest.

The tidal prisms and residual volume fluxes across all transects marked in Figure 7 are shown in Figures 10 and 11. The largest tidal prisms are observed in the Dutch Wadden Sea with values above or slightly below $10^9 m^3$. The reason for these high values is simply the large area extent of the Wadden Sea basins in the Dutch Wadden Sea. Also in the North Frisian Wadden Sea some of the inlets show large tidal prisms with values around $5 \cdot 10^8\ m^3$, such as for the Sylt-Rømø bight (through the Lister Dyb), through the Hörnum Tief and the Heverstrom. In contrast, tidal prisms are small (below $2 \cdot 10^8\ m^3$) for the comparably narrow East Frisian Wadden Sea. The values of the tidal prisms stated here are long-term mean values; for individual tidal periods, the prism typically varies within a range of about 20% [*Duran-Matute et al.*, 2014].

The residual flows in the Wadden Sea show consistently the anticlockwise circulation of the German Bight. With the exception of the first westernmost inlets (the Marsdiep and the Eierlands Gat), residual currents are directed eastward in the Dutch Wadden Sea, with high values between 200 and 500 $m^3\ s^{-1}$ across the watersheds between some of the islands and the mainland. These residual flows are comparable to discharges of the large rivers during the same period (Elbe: 769 $m^3\ s^{-1}$, Weser: 245 $m^3\ s^{-1}$, see Figure 10b).

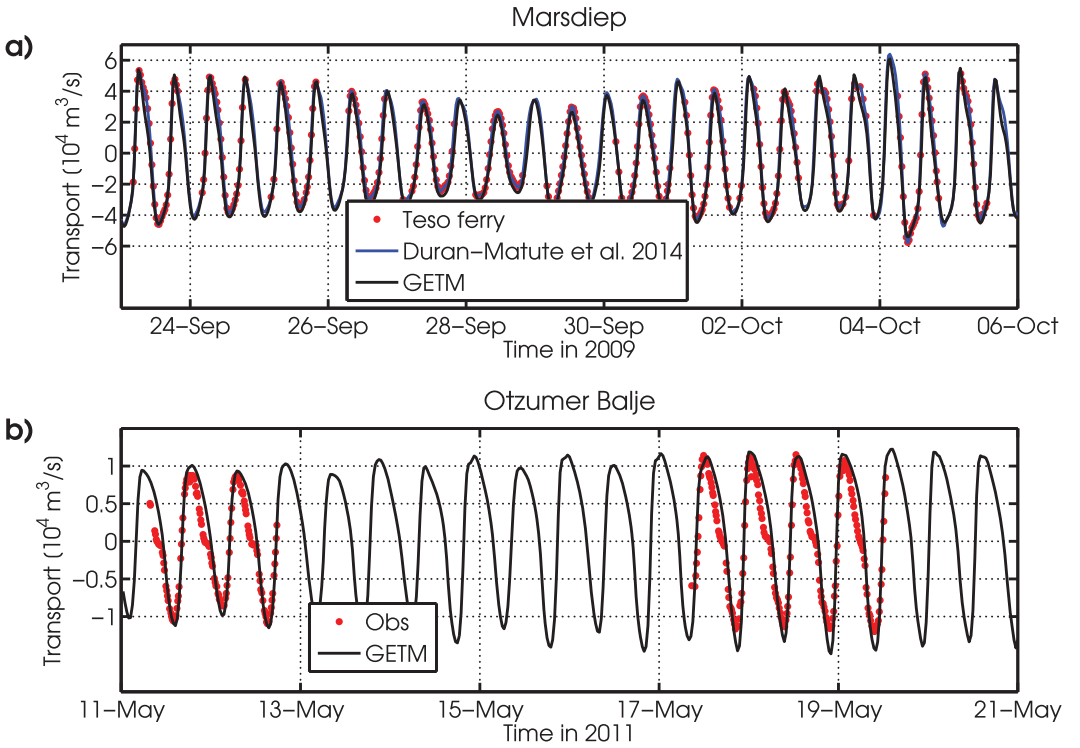

Figure 8. Comparison between observed and simulated volume fluxes through two tidal inlets. (a) Marsdiep (with model results by *Duran-Matute et al.* [2014] and from the present study); (b) Otzumer Balje. See Figure 7 for the location of the inlets.

The major drivers are the coastal current baroclinically driven by river discharges, the residual current driven by the Kelvin-wave-type tidal dynamics, and the wind and waves from predominantly westerly directions. The strong eastward residual flow continues into the East Frisian Wadden Sea (with 551 m^3 s^{-1} across the watershed south of the island of Juist), but then the water seems to leave the Wadden Sea through the

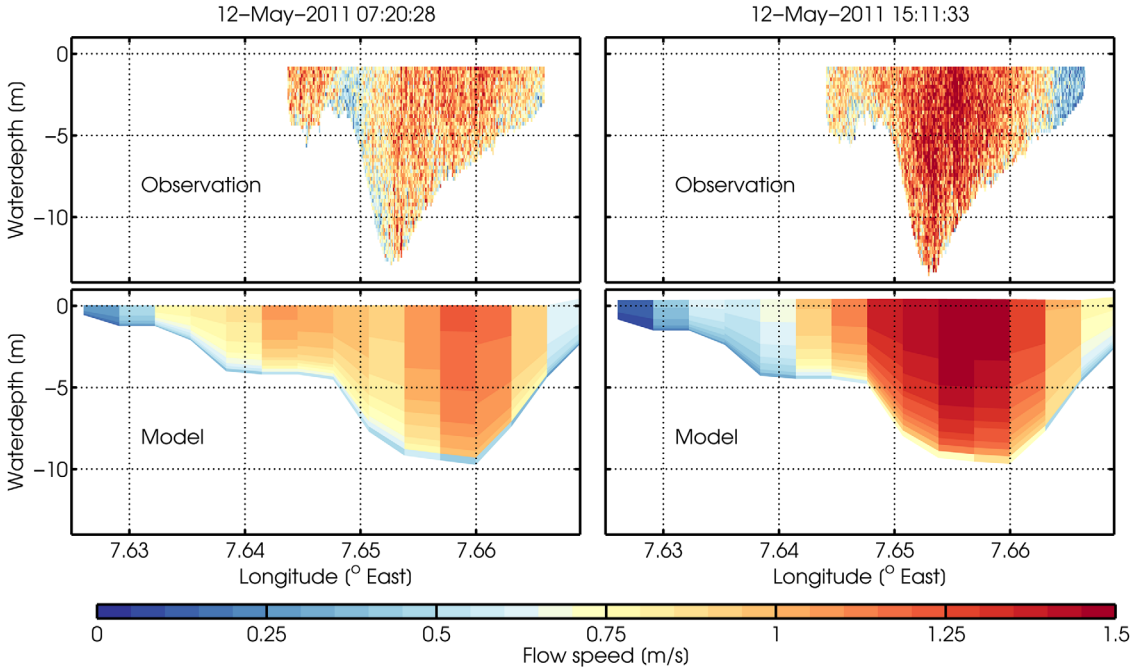

Figure 9. Comparison between observed and simulated current speed along a transect across the Otzumer Balje tidal inlet between the islands of Langeoog and Spiekeroog at two instants of time.

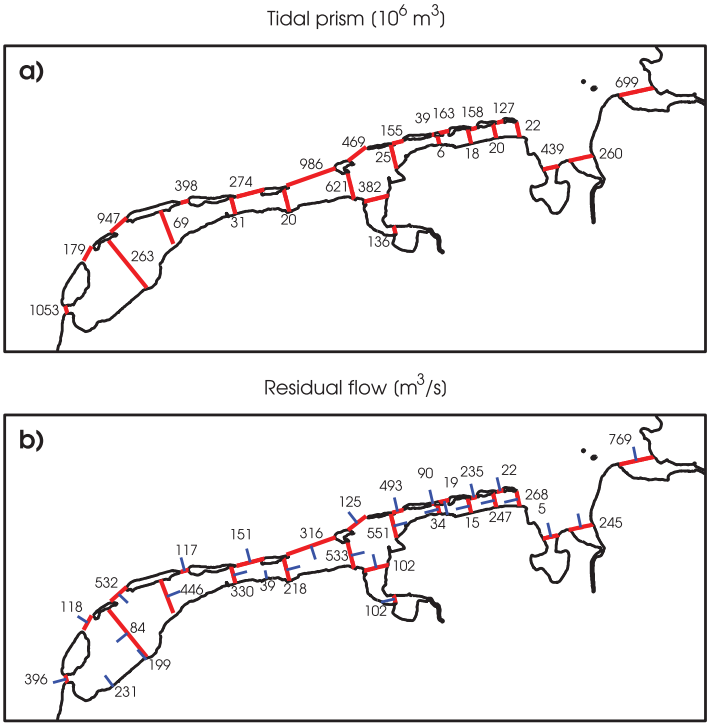

Figure 10. Simulated annual mean tidal prisms (in m^3 s−1) of selected basins (upper top) and residual fluxes (in m^3 s−1) across selected transects (bottom) for the southern Wadden Sea. The short blue lines indicate the direction of the residual flow.

Norderneyer Seegat into the North Sea. The residual currents are then directed westward in the narrow eastern part of the East Frisian Wadden Sea, seemingly fed by the Weser discharge. In the North Frisian Wadden Sea (Figure 11), residual flows are generally directed northward, again following the anticlockwise circulation of the German Bight. The flow entering the Heverstrom at a rate of >300 m^3 s^{-1} exits the Wadden Sea through the Hörnum Tief, since the Hindenburg Dam between the island of Sylt and the mainland builds a barrier further northward. The residual flow through the Lister Dyb simply equals the local freshwater balance (5 m^3 s^{-1}) in the Sylt-Rømø bight. Northward, in the Danish Wadden Sea a northward through-flow of about 160 m^3 s^{-1} is calculated. Finally, we reiterate the point made in section 3.4, that annual mean values of residual transport can vary strongly from year to year, even in sign; the values listed here are specifically for the years 2009–2011.

4.2. Eulerian Residual Circulation

The Eulerian residual circulation is calculated here as the Eulerian residual transport velocity (projected to a prescribed along-channel direction) $\langle u\rangle$, which is the tidally averaged, vertically resolved velocity along σ coordinates, weighted by the changing water depth D:

$$\langle u(x,y,\sigma,t)\rangle = \frac{\int_{t-T/2}^{t+T/2} u(x,y,\sigma,\tau)D(x,y,\tau)\,\mathrm{d}\tau}{\int_{t-T/2}^{t+T/2} D(x,y,\tau)\,\mathrm{d}\tau}, \tag{1}$$

where T is the tidal period. In (1), the averaging is carried out in a way that the cross-sectional integral of $\langle u\rangle$ exactly gives the residual flow (see section 4.1). The Eulerian residual transport velocity reflects estuarine circulation processes in the Wadden Sea such as net inflow near the bottom and net outflow near the surface for a Wadden Sea being less dense than the North Sea [see, e.g., *Burchard and Badewien*, 2015].

The strength of the estuarine circulation is quantified by a measure which gives an estuarine circulation value of $\mathcal{M}(\langle u\rangle)=u_e$ for a landward flow of u_e in the lower half of the water column and a seaward flow of $-u_e$ in the upper half of the water column [see *Burchard et al.*, 2011]:

$$\mathcal{M}(\langle u\rangle) = -\frac{1}{W}\int_0^W \frac{4}{\langle D(y,t)\rangle^2}\int_{-1}^0 \langle u(y,\sigma,t)\rangle\left(\sigma+\frac{1}{2}\right)\mathrm{d}\sigma\,\mathrm{d}y. \tag{2}$$

where y is the direction along the transect, $\langle D\rangle$ is the tidally averaged water depth, and W is the length of the transect. Negative values of $\mathcal{M}(\langle u\rangle)$ represent inverse estuarine circulation (net outflow at the bottom).

The strength of the Eulerian residual transport velocity is calculated and discussed here for selected transects across tidal channels in the Wadden Sea (see Figure 12). The focus of the analysis is the dependence of

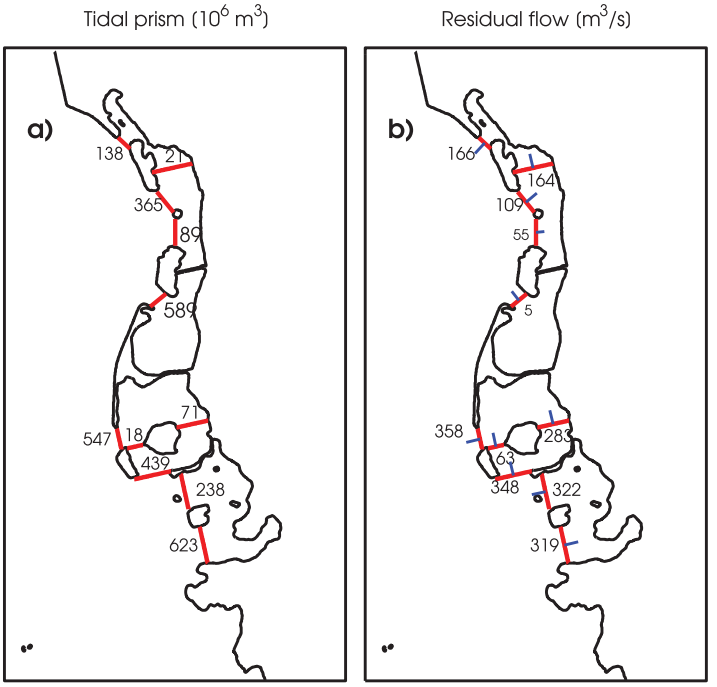

Figure 11. Simulated annual mean tidal prisms (in m^3 s−1) of selected basins (left) and residual fluxes (in m^3 s−1) across selected transects (right) for the northern Wadden Sea. The short blue lines indicate the direction of the residual flow.

$\mathcal{M}(\langle u \rangle)$ on the cross-sectionally averaged horizontal density gradient $\partial_\perp \rho$ and the wind stress $\tau_\perp$, both projected to the along-channel direction, with positive values landward into the Wadden Sea. It can be seen from Figure 12 that there is a large diversity of patterns for the sensitivity of estuarine exchange flow to external forcing. For most inlets, a less dense Wadden Sea generally results in classical estuarine circulation as seen for example for the Marsdiep, the Jade, and the Hörnum Tief. Some of the inlets show high values of estuarine circulation of up to $\mathcal{M}(\langle u \rangle)$=0.1 m s^{-1} (e.g., Pinke Gat) at strong density gradient forcing ($\partial_\perp \rho < -3 \cdot 10^{-4}$ kg m^{-4}). In some inlets, strong inverse estuarine circulation occurs, when the density gradient forcing reverses, such as for the Lister Dyb, where values of $\mathcal{M}(\langle u \rangle) < -0.05$ m s^{-1} occur. Such density gradient reversals can occur due to cooling of the Wadden Sea in autumn [*Burchard et al*., 2008; *Burchard and Badewien*, 2015] strong evaporation during summer [*Onken and Riethmüller*, 2010] or strong discharge of upstream rivers [*Flöser et al*., 2011]. In some of the North Frisian/Danish inlets (Hörnum Tief, Lister Dyb, Graadyb), a significant wind straining effect can be seen (as already shown by *Purkiani et al*. [2016] in a more detailed study for the Lister Dyb): strong wind stress directed into the Wadden Sea decreases or reverses estuarine circulation, but this effect can also be seen in the Marsdiep (compare to *Duran-Matute et al*. [2014]). The exchange flow reversals are more throughly discussed when analyzing time series of Total Exchange Flow in section 4.3. Some of the inlets show a less clear response to external forcing. In the Süderaue, no clear dependence on density gradient forcing is visible and strong wind stress in general (landward and seaward) causes weakening or reversal of the estuarine circulation. For the Otzumer Balje (where the spatial resolution of the model seems to be too coarse, see section 4.1), no clear relation to forcing is visible. The detailed study of some of the more narrow or complex individual inlets would require additional locally nested models with higher spatial resolution (e.g., $\Delta x \leq 100$ m) [see *Purkiani et al*., 2015, 2016].

Finally, the influence of tidal straining on estuarine circulation tidal asymmetry is quantified by means of inspecting the dependence of the tidally and cross-sectionally averaged ratio of tidally averaged covariance of eddy viscosity with vertical shear and tidally averaged eddy viscosity, $\langle A_v' \partial_z u' \rangle / \langle A_v \rangle$ on wind stress and horizontal buoyancy gradients. This ratio is a key element of the tidal straining estuarine circulation in tidally energetic inlets such as in the Wadden Sea [see *Burchard et al*., 2011]. This mechanism is characterized by high values of eddy viscosity during flood (positive shear) and low values during ebb (negative shear), such that a positive covariance is indicative for tidal straining. Figure 13 shows this ratio. The picture is much less clear than for the intensity of the estuarine circulation. One reason may be that lateral circulation patterns in tidal inlets may lead to an increase of vertical stratification and thus to a decrease of eddy viscosity already during full flood [*Becherer et al*., 2011; *Purkiani et al*., 2015; *Schulz et al*., 2015]. Still, in some of the inlets, an increase of tidal asymmetry with increased density gradient forcing can be seen (Marsdiep, Hörnum Tief, Jade). In the Marsdiep, the Otzumer Balje and the Graadyb also a significant reduction of the tidal asymmetry with increased landward wind forcing is visible.

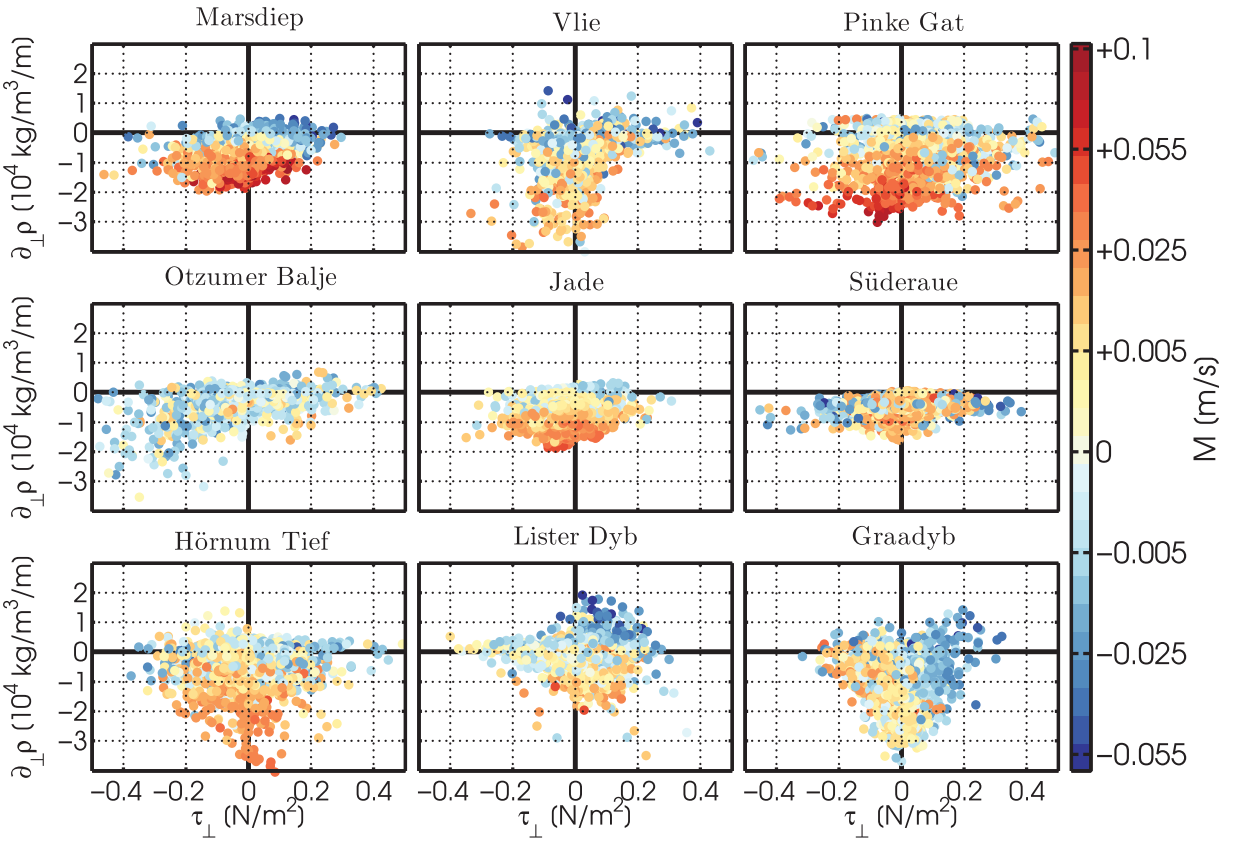

Figure 12. Scatter plot for the intensity of estuarine circulation intensity $\mathcal{M}$ (color code) as function of the wind stress orthogonal to the transect (positive for wind stress oriented toward land) and horizontal buoyancy gradient (positive for higher buoyancy toward land).

4.3. Total Exchange Flow

In order obtain a deeper insight into estuarine exchange flow, *MacCready* [2011] developed the concept of total exchange flow (TEF), based on the isohaline framework proposed by *MacCready et al.* [2002]. The volume transport Q through the cross-sectional area A_s which has a salinity above a specific value s is defined as

$$Q(s) = \left\langle \int_{A_s} u \, \mathrm{d}A \right\rangle. \tag{3}$$

Note that $u > 0$ when directed landward. In addition, we define

$$Q_{in} = \left\langle \int_{A_+} u \, \mathrm{d}A \right\rangle; \quad Q_{out} = -\left\langle \int_{A_-} u \, \mathrm{d}A \right\rangle \tag{4}$$

as the inflowing and outflowing water volume transport through tidal inlets, with A_+ and A_- being the cross-sectional subareas with inflowing water and outflowing water, respectively. With this, $Q(0) = Q_{in} - Q_{out}$, since the area with salinities larger than $s = 0$ always covers the entire cross-section, and $Q(s_{\max}) = 0$ with the maximum ocean salinity $s_{\max}$. Representative inflow salinity, s_{in}, and outflow salinity, s_{out} can be defined as

$$s_{in} = \frac{1}{Q_{in}} \left\langle \int_{A_+} su \, \mathrm{d}A \right\rangle; \quad s_{out} = -\frac{1}{Q_{out}} \left\langle \int_{A_-} su \, \mathrm{d}A \right\rangle, \tag{5}$$

see *MacCready* [2011]. The exchange flow characteristics Q_{in}, Q_{out}, s_{in}, and s_{out} are consistent with the *Knudsen* [1900] theorem based on volume and salt conservation, see also the review by *MacCready and Geyer* [2010]. An exchange flow as function of the salinity is then obtained by differentiating Q with respect to s:

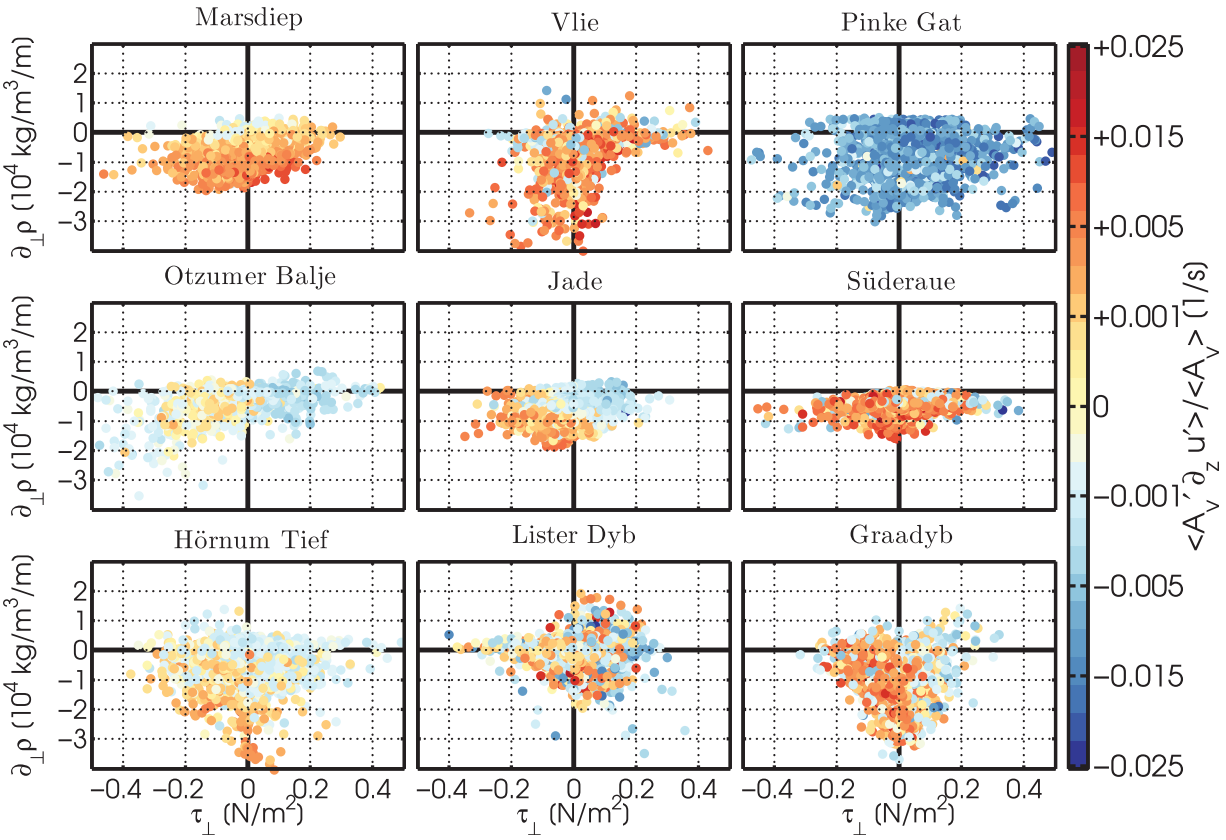

Figure 13. Scatter plot of the tidally and cross-sectionally averaged ratio of tidally averaged covariance of eddy viscosity with vertical shear and tidally averaged eddy viscosity, $\langle A_v' \partial_z u' \rangle / \langle A_v \rangle$, as function of the wind stress orthogonal to the transect (positive for wind stress oriented toward land) and horizontal buoyancy gradient (positive for higher buoyancy toward land).

$$q(s) = \frac{\partial Q(s)}{\partial s}. \tag{6}$$

Sutherland et al. [2011] have used this relation to characterize the total exchange flow for the Salish Sea. The advantage of the TEF over classical calculations of exchange flows is that it gives a one-dimensional (with salinity as independent coordinate) view of complex exchange flow across a transect. As discussed by *Purkiani et al.* [2016], the strength of the Eulerian estuarine circulation, $\mathcal{M}(\langle u \rangle)$ defined in section 4.2, which gives a measure for the tidally averaged vertical overturning, is useful for drawing conclusions for residual transport of SPM. $\mathcal{M}(\langle u \rangle)$ quantifies the near-bed landward residual flow, which is partially responsible for the landward SPM transport. In addition, tidal SPM pumping is driven by tidal asymmetries which are partially a consequence of estuarine circulation. In contrast to $\mathcal{M}(\langle u \rangle)$, TEF is additionally accounting for lateral exchange flow which can be driven for example by flow curvature and other bathymetric asymmetries, or by lateral density gradients, but it does not indicate the potential for net SPM transport.

The Total Exchange Flow is shown as time series profile plots (Figure 14) and as corresponding time series plots of bulk exchange flow quantities (Figure 15) for the Lister Dyb, the Otzumer Balje, and the Marsdiep during the year 2010.

The Lister Dyb between the islands of Sylt and Rømø shows a clear annual cycle in mean salinity with high values (>33 psu) during summer due to strong evaporation [see, e.g., *Burchard et al.*, 2008; *Onken and Riethmüller*, 2010] and low values (<30 psu) during winter and spring due to strong runoff (Figures 14a and 15a). The salinity in Lister Dyb may additionally be significantly influenced by the discharge of the Elbe river into the German Bight. The freshwater plume is feeding the coastal current off the North Frisian coast and may even lead to lower offshore salinities [*Flöser et al.*, 2011]. In Lister Dyb, the inflow of waters mostly occurs at higher salinities than the outflows ($s_{in} > s_{out}$, see Figure 15a), which is the typical situation in humid regions. However, occasionally the inflow occurs at lower salinities than the outflow ($s_{in} < s_{out}$, see

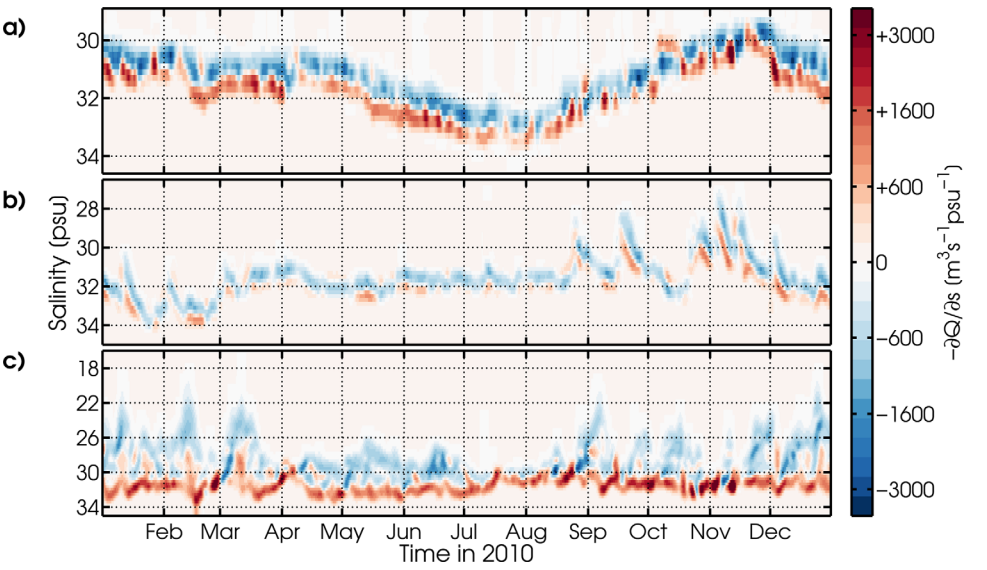

Figure 14. Total exchange flow (TEF) $\partial Q/\partial s$ across (a) Lister Dyb (between Sylt and Rømø), (b) Otzumer Balje (between Langeoog and Spiekeroog), (c) and Marsdiep (between mainland and Texel) during the year 2010. Note the nonlinear scaling of the color coding. Positive values indicate inflow.

Figure 15a), as for example during a 2 week period in October 2010. Figure 2 shows that during this period winds were weak and south-easterly, but a high discharge event from the Elbe River of up to 2000 $m^3\ s^{-1}$ was recorded, lowering the salinity offshore from the North Frisian islands, and reversing the buoyancy gradient in the inlet (as reported by *Flöser et al.* [2011] for April 2006). Some other reversals in the Lister Dyb can be attributed to westerly wind directions, such as during early April and late August 2010, see Figures 2a and 2b. These would generate sufficient wind straining pushing surface waters toward the coast, such that bottom waters show a compensating seaward residual flow. This so-called wind straining

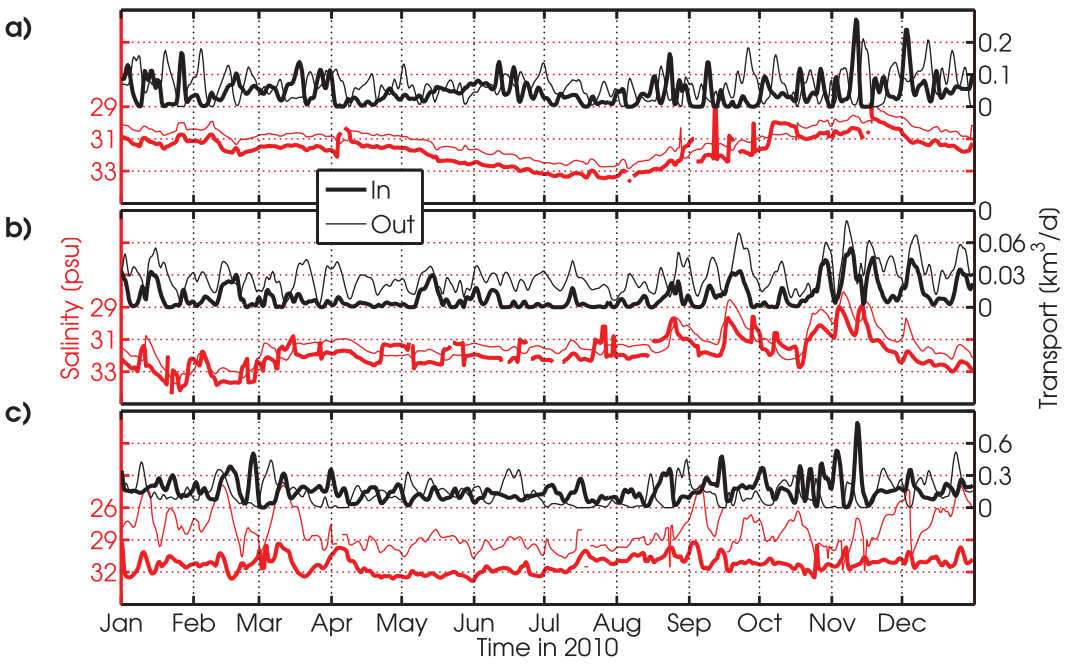

Figure 15. Inflow (bold lines) and outflow (thin lines) salinity (red) and transport (black) across three tidal inlets in the Wadden Sea during the year 2010 according to the *Knudsen* [1900] theorem, see equations (4) and (5). (a) Lister Dyb (between Sylt and Rømø), (b) Otzumer Balje (between Langeoog and Spiekeroog), (c) Marsdiep (between mainland and Texel). The salinity time series are interrupted at times, when the corresponding inflow or outflow vanishes.

[*Scully et al*., 2005] has recently been shown by *Purkiani et al*. [2016] to regularly cause reversal of estuarine circulation in the Lister Dyb. In the Lister Dyb, there are also some periods, when the outflow part of the tidally averaged salt transport is fully compensated by an inflow part, such that TEF only shows inflow of salt (e.g., in late January 2010). Also the opposite occurs occasionally, e.g., in early February 2010, when TEF shows only outflow of salt. Since the Lister Dyb is the only connection of the Sylt-Rømø bight to the North Sea, this means that the total salt mass inside the Sylt-Rømø bight is increasing (or decreasing), which either means a water volume increase at the same mean salinity or an increased mean salinity at unchanged water volume, or a combination of both.

The situation in Otzumer Balje (between the islands of Langeoog and Spiekeroog) is completely different (Figure 14b and 15b). The annual cycle is less clear, with lowest salinities in autumn and highest salinities in late winter and early spring. It has already been shown by *Burchard and Badewien* [2015] that there is a strong interannual variability in the seasonality of salinity in the Otzumer Balje. In addition to the freshwater runoff from land, and as a difference to the Lister Dyb, the Otzumer Balje with its relatively small tidal prism could be influenced by coastal upwelling and downwelling due to westerly or easterly winds along the East Frisian coast which is facing northward. Due to the small tidal prism and the connection to adjacent tidal basins through water sheds behind the neighboring islands, the short-term variability of the salinity is much higher in the Otzumer Balje than in the much larger Sylt-Rømø bight. Outflow of water masses through the Otzumer Balje clearly dominates, which is explained by the annually averaged volume outflow of 235 $m^3\ s^{-1}$, see Figure 10b. Occasional short-term reversals of estuarine circulation are also visible for the Otzumer Balje, which may occur due to reversals of the buoyancy gradient, such as in August 2010, as reported by *Burchard and Badewien* [2015], see Figure 15b.

Also the Marsdiep has its own characteristic Total Exchange Flow pattern (Figures 14c and 15c). The mean salinity is relatively stable without a clear annual cycle with values around 30 psu. There is typically a strong classical estuarine circulation with inflow at about 32 psu and outflow over the wide range of 22–31 psu. This broad outflow pattern can be explained by the strong and direct influence of variable freshwater discharge from the Lake IJssel into the southern part of the Western Dutch Wadden Sea [see *Duran-Matute et al*., 2014]. One typical example for a freshwater-driven outflow peak is visible in early September 2010, when a strong discharge event is recorded (Figure 2d), and consequently a broad low salinity (ranging from 20 to 30 psu, with $s_{out} \approx 24$ psu) outflow is observed. At times, multiple inflow peaks at different salinities occur due to the more complex hydrographic structure of the Marsdiep, as already discussed by *Zimmerman* [1976]; *Buijsman and Ridderinkhof* [2008].

5. Conclusions

For the first time, a baroclinic numerical model for the entire Wadden Sea is presented which resolves the dynamics in all major tidal channels and intertidal flats. This allows for a quantitative analysis of the regional characteristics and differences across the entire Wadden Sea. This excludes systematic errors which are otherwise introduced by comparing local models of different tidal basins simulated by different models using different forcings and different bathymetric data. Setting up such a complex model simulation is quite challenging. One problem is that quite an amount of bathymetry smoothing is needed to get stable model runs. Instabilities are typically caused by the drying and flooding, most pronounced at the transitions from the steep channels to the tidal flats. During the development of the setup, we corrected some of the numerics in GETM, including a more consistent treatment of the layer thicknesses and the transition from the full hydrodynamics to the reduced physics at the dry tidal flats [see *Burchard et al*., 2004]. This helped us to reverse some bathymetry smoothing applied at the initial stage. Another challenge in the setup development was to correctly estimate and distribute river discharges.

The model assessment shows a high model skill for comparison with various data sets. Most importantly, tidal gauge data in the Wadden Sea are well-reproduced, due to the nesting of the Wadden Sea model into a hierarchy of larger-scale models. This allows for a consideration of remote forcing effects to the Wadden Sea dynamics. Specifically important is here the good reproduction of the M_4 tidal constituent which is responsible for a large part of the net sediment transport in the Wadden Sea [*Gräwe et al*., 2014]. Also hydrographic data are sufficiently well-reproduced with correlations coefficients generally larger than 0.7. The proper representation of hydrographic data is a precondition for the reproduction of effects of tidal

straining due to horizontal density gradients, a process which is a substantial driver of sediment flux into the Wadden Sea and other tidally energetic inlets [*Scully and Friedrichs*, 2007; *Burchard et al*., 2008, 2013]. A direct assessment of the seasonal variability of the density gradients toward the Wadden Sea was provided by data obtained from a ship of opportunity regularly commuting between Büsum and Helgoland during the summer season. These data demonstrate that the reversal of the temperature gradient after summer is well-reproduced, as well as temporal variations in the salinity gradient. For the same region (east of Helgoland), subtidal variability of surface currents as response to the variability of wind forcing could be well reproduced by the model. For volume fluxes through tidal gullies, only a few observations are available (Marsdiep and Otzumer Balje). For the relatively deep and wide Marsdiep observed data are reproduced in much detail, and volume fluxes through the narrow Otzumer Balje (about 500 m width below 5 m mean depth) are also reproduced in terms of amplitude and phase. However, for the latter inlet, the spatial resolution of $\Delta x = 200$ m seems to be insufficient to reproduce details of the tidal flow in that inlet.

With this, a validated three-dimensional baroclinic model of the entire Wadden Sea is available for the first time, allowing for the comparative quantitative assessment of local differences between various tidal inlets.

First analysis of the model results generated a consistent map of tidal prisms and residual volume fluxes for the entire Wadden Sea, represented by the conditions during the years 2009–2011. As a result, residual fluxes generally follow the anticlockwise circulation in the German Bight in a way that residual transports across water sheds between the islands and the mainland are generally eastward in the Dutch Wadden Sea and the western part of the East Frisian Wadden Sea and northward in the North Frisian Wadden Sea. Exceptions are the eastern part of the narrow East Frisian Wadden Sea and the waters around the islands of Sylt and Rømø which are connected to the mainland by artificial dams. A further exception is the Marsdiep, which is directly affected by freshwater discharge from Lake IJssel.

A first analysis of estuarine circulation shows that the Eulerian residual transport velocity profiles are generally highly correlated to density gradients and wind stress into the Wadden Sea, but the temporal variability is very high. Tidal inlets in the North Frisian Wadden Sea respond to wind forcing in a highly correlated way, with reversals of estuarine circulation during periods of strong westerly winds. The reason for this is probably the orientation of these inlets toward to main westerly wind direction. This correlation is less clear in the Dutch Wadden Sea (with the exception of the Marsdiep which is oriented toward the major westerly wind directions) and the East Frisian Wadden Sea, since the orientation of the inlets is more in north-south direction. The expected correlation between the eddy-viscosity with shear covariance and density gradient forcing or wind stress forcing is relatively weak in many inlets, indicating that often probably other mechanisms play a dominant role in driving estuarine circulation. There are various explanations for such deviations from theory: For the case of the Sylt-Rømø bight, *Purkiani et al*. [2015] could show for example that a combination of channel curvature and convergence can lead to a complex combination of lateral and vertical residual shear which is not directly connected to longitudinal density gradients. By means of idealized simulations, *Schulz et al*. [2015] demonstrated that in tidally energetic channel flow due to lateral circulation vertical shear and stratification may be stronger during flood than during ebb, other than assumed for classical tidal flow. However, in several inlets a clear correlation of tidal straining with wind stress, longitudinal buoyancy gradient or both is visible.

In contrast to the Eulerian analysis which is indicative for the direction of the subtidal SPM transport (landward for positive $\mathcal{M}$), the TEF analysis gives direct insights into the dependence of the estuarine exchange flow on freshwater forcing. Freshwater pulses from inside the tidal basin (such as discharge peaks from Lake Ijssel) into the Marsdiep are visible as peaks of the outflow transport Q_{out} and minima of the outflow salinity s_{out}. Freshwater forcing from seaward of the tidal inlet (as for example seen for the Lister Dyb during freshwater discharge pulses from the Elbe River) may reverse $\mathcal{M}$ by changing the sign of the longitudinal buoyancy gradient, only if the vertical overturning circulation is affected. In the TEF analysis, such an event is directly lowering the inflow salinity to values below the outflow salinity, also when the exchange flow is dominated by lateral shear.

As a result, a validated three-dimensional baroclinic model for the entire Wadden Sea is available now in high-resolution and good accuracy. This model constitutes a solid basis for analyzing fluxes of suspended particulate matter and biogeochemical compounds between the Wadden Sea and the adjacent North Sea.

Acknowledgments
The present study has been jointly funded by the German Federal Ministry of Research and Education (BMBF) and the Netherlands Organisation for Scientific Research (NWO) in the framework of the project PACE (The future of the Wadden Sea sediment fluxes: still keeping pace with sea level rise?). In Germany, the project identification number was FKZ 03F0634A and in the Netherlands, this project was ZKO-project #839.11.003. The work of Theo Gerkema has been additionally supported by a visiting scientist grant through IOW. The numerical simulations have been carried out on supercomputers of the North-German Supercomputing Alliance (HLRN). The authors are grateful to Knut Klingbeil (Rostock, Germany) for the code maintenance of GETM and technical support. We furthermore thank Thorbjørn Andersen (Copenhagen, Denmark) for observational data in the Lister Dyb. The observational data on which this study is based are available by request to the corresponding author (hans.burchard@io-warnemuende.de). The model output for the simulation of the entire Wadden Sea can be requested from the first author (ulf.graewe@io-warnemuende.de).

References

Banas, N. S., B. M. Hickey, J. A. Newton, and J. L. Ruesink (2007), Tidal exchange, bivalve grazing, and patterns of primary production in Willapa Bay, Washington, USA, *Mar. Ecol. Prog. Ser.*, *341*, 123–139.

Becherer, J., H. Burchard, G. Flöser, V. Mohrholz, and L. Umlauf (2011), Evidence of tidal straining in well-mixed channel flow from microstructure observations, *Geophys. Res. Lett.*, *38*, L17611, doi:10.1029/2011GL049005.

Becherer, J., M. Stacey, L. Umlauf, and H. Burchard (2015), Lateral circulation generates flood-tide stratification and estuarine exchange flow in a curved channel, *J. Phys. Oceanogr.*, *44*, 638–656.

Buijsman, M. C., and H. Ridderinkhof (2007), Long-term ferry-ADCP observations of tidal currents in the Marsdiep inlet, *J. Sea Res.*, *57*, 237–256.

Buijsman, M. C., and H. Ridderinkhof (2008), Variability of secondary currents in a weakly stratified tidal inlet with low curvature, *Cont. Shelf Res.*, *28*, 1711–1723.

Burchard, H., and T. H. Badewien (2015), Thermohaline residual circulation of the Wadden Sea, *Ocean Dyn.*, *65*, 1717–1730.

Burchard, H., and K. Bolding (2002), GETM: A general estuarine transport model, Scientific documentation, *Tech. Rep. EUR 20253 EN, Eur. Comm.*, Ispra, Italy.

Burchard, H., K. Bolding, and M. R. Villarreal (2004), Three-dimensional modelling of estuarine turbidity maxima in a tidal estuary, *Ocean Dyn.*, *54*, 250–265.

Burchard, H., G. Flöser, J. V. Staneva, R. Riethmüller, and T. Badewien (2008), Impact of density gradients on net sediment transport into the Wadden Sea, *J. Phys. Oceanogr.*, *38*, 566–587.

Burchard, H., R. D. Hetland, E. Schulz, and H. M. Schuttelaars (2011), Drivers of residual circulation in tidally energetic estuaries: Straight and irrotational estuaries with parabolic cross-section, *J. Phys. Oceanogr.*, *41*, 548–570.

Burchard, H., H. M. Schuttelaars, and W. R. Geyer (2013), Residual sediment fluxes in weakly-to-periodically stratified estuaries and tidal inlets, *J. Phys. Oceanogr.*, *43*, 1841–1861.

Dissanayake, D. M. P. K., R. Ranasinghe, and J. A. Roelvink (2012), The morphological response of large tidal inlet/basin systems to relative sea level rise, *Clim. Change*, *113*, 252–276.

Duran-Matute, M., and T. Gerkema (2015), Calculating residual flows through a multiple-inlet system: The conundrum of the tidal period, *Ocean Dyn.*, *65*, 1461–1475.

Duran-Matute, M., T. Gerkema, G. J. de Boer, J. J. Nauw, and U. Gräwe (2014), Residual circulation and freshwater transport in the Dutch Wadden Sea: A numerical modelling study, *Ocean Sci.*, *10*, 611–632.

Flöser, G., H. Burchard, and R. Riethmüller (2011), Observational evidence for estuarine circulation in the German Wadden Sea, *Cont. Shelf Res.*, *31*, 1633–1639.

Gräwe, U., H. Burchard, M. Müller, and H. M. Schuttelaars (2014), Seasonal variability in M_2 and M_4 tidal constituents and its implications for the coastal residual sediment transport, *Geophys. Res. Lett.*, *41*, 5563–5570, doi:10.1002/2014GL060517.

Gräwe, U., P. Holtermann, K. Klingbeil, and H. Burchard (2015), Advantages of vertically adaptive coordinates in numerical models of stratified shelf seas, *Ocean Modell.*, *92*, 56–68.

Herrling, G., and C. Winter (2014), Morphological and sedimentological response of a mixed-energy barrier island tidal inlet to storm and fair-weather conditions, *Earth Surf. Dyn.*, *2*, 363–382.

Herrling, G., and C. Winter (2015), Tidally- and wind-driven residual circulation at the multiple-inlet system East Frisian Wadden Sea, *Cont. Shelf Res.*, *106*, 45–59.

Hofmeister, R., H. Burchard, and J.-M. Beckers (2010), Non-uniform adaptive vertical grids for 3D numerical ocean models, *Ocean Modell.*, *33*, 70–86.

Knudsen, M. (1900), Ein hydrographischer Lehrsatz, *Ann. Hydrogr. Mar. Meteorol.*, *28*, 316–320.

Kondo, J. (1975), Air-sea bulk transfer coefficients in diabatic conditions, *Boundary Layer Meteorol.*, *9*, 91–112.

Kowalski, N., O. Dellwig, M. Beck, M. Grunwald, C.-D. Dürselen, T. Badewien, H. Brumsack, J. van Beusekom, and M. Böttcher (2012), A comparative study of manganese dynamics in the water column and sediments of intertidal systems of the North Sea, *Estuarine Coastal Shelf Sci.*, *100*, 3–17.

Lettmann, K. A., J.-O. Wolff, and T. H. Badewien (2009), Modelling the impact of wind and waves on suspended particulate matter fluxes in the East Frisian Wadden Sea (Southern North Sea), *Ocean Dyn.*, *59*, 239–262.

MacCready, P. (2011), Calculating estuarine exchange flow using isohaline coordinates, *J. Phys. Oceanogr.*, *41*, 1116–1124.

MacCready, P., and W. R. Geyer (2010), Advances in estuarine physics, *Annu. Rev. Mar. Sci.*, *2*, 35–58.

MacCready, P., R. D. Hetland, and W. R. Geyer (2002), Long-term isohaline salt balance in an estuary, *Cont. Shelf Res.*, *22*, 1591–1601.

Nauw, J., L. Merckelbach, H. Ridderinkhof, and H. van Aken (2014), Long-term ferry-based observations of the suspended sediment fluxes through the Marsdiep inlet using acoustic Doppler current profilers, *J. Sea Res.*, *87*, 17–29.

Onken, R., and R. Riethmüller (2010), Determination of the freshwater budget of tidal flats from measurements near a tidal inlet, *Cont. Shelf Res.*, *30*, 924–933.

Postma, H. (1982), *Hydrography of the Wadden Sea: Movements and Properties of Water and Particulate Matter*, 75 pp., A. A. Balkema.

Purkiani, K., J. Becherer, G. Flöser, U. Gräwe, V. Mohrholz, H. M. Schuttelaars, and H. Burchard (2015), Numerical analysis of stratification and de-stratification processes in a tidally energetic inlet with an ebb tidal delta, *J. Geophys. Res. Oceans*, *120*, 225–243, doi:10.1002/2014JC010325.

Purkiani, K., J. Becherer, K. Klingbeil, and H. Burchard (2016), Wind-induced variability of estuarine circulation in a tidally energetic inlet with curvature, *J. Geophys. Res. Oceans*, *121*, 29, doi:10.1002/2015JC010945.

Reise, K., M. Baptist, P. Burbridge, N. Dankers, L. Fischer, B. Flemming, A. P. Oost, and C. Smit (2010), The Wadden Sea: A universally outstanding tidal wetland, *Wadden Sea Ecosystem No. 29*, technical report, Common Wadden Sea Secr., Wilhelmshaven, Germany. [Available at http://www.waddensea-secretariat.org/sites/default/files/downloads/the-waddensea- 2010-part1.pdf.]

Saha, S., S. Moorthi, H.-L. H. Pan, X. Wu, J. Wang, S. Nadiga, P. Tripp, R. Kistler, J. Woollen, and D. Behringer (2010), The NCEP climate forecast system reanalysis, *Bull. Am. Meteorol. Soc.*, *91*, 1015–1057.

Sassi, M., M. Duran-Matute, T. van Kessel, and T. Gerkema (2015), Variability of residual fluxes of suspended sediment in a multiple tidal-inlet system: The Dutch Wadden Sea, *Ocean Dyn.*, *65*, 1321–1333.

Sassi, M., T. Gerkema, M. Duran-Matute, and J. J. Nauw (2016), Residual water transport in the Marsdiep tidal inlet inferred from observations and a numerical model, *J. Mar. Res.*, *74*, 21–42.

Schulz, E., H. M. Schuttelaars, U. Gräwe, and H. Burchard (2015), Impact of the depth-to-width ratio of a tidally energetic estuary on the residual circulation, *J. Phys. Oceanogr.*, *45*, 2048–2069.

Scully, M. E., and C. T. Friedrichs (2007), Sediment pumping by tidal asymmetry in a partially mixed estuary, *J. Geophys. Res.*, *112*, C07028, doi:10.1029/2006JC003784.

Scully, M. E., C. T. Friedrichs, and J. M. Brubaker (2005), Control of estuarine stratification and mixing by wind-induced straining of the estuarine density field, *Estuaries*, *28*, 321–326.

Stanev, E. V., J.-O. Wolff, H. Burchard, K. Bolding, and G. Flöser (2003), On the circulation in the East Frisian Wadden Sea: Numerical modelling and data analysis, *Ocean Dyn.*, *53*, 27–51.

Stanev, E. V., F. Ziemer, J. Schulz-Stellenfleth, J. Seemann, J. Staneva, and K.-W. Gurgel (2015), Blending surface currents from HF radar observations and numerical modeling: Tidal hindcasts and forecasts, *J. Atmos. Oceanic Technol.*, *32*, 256–281.

Staneva, J., E. V. Stanev, J.-O. Wolff, T. H. Badewien, R. Reuter, B. Flemming, A. Bartholomä, and K. Bolding (2009), Hydrodynamics and sediment dynamics in the German Bight. A focus on observations and numerical modelling in the East Frisian Wadden Sea, *Cont. Shelf Res.*, *29*, 302–319.

Sutherland, D., P. MacCready, N. S. Banas, and L. F. Smedstad (2011), A model study of the Salish Sea estuarine circulation, *J. Phys. Oceanogr.*, *41*, 1125–1143.

Umlauf, L., and H. Burchard (2005), Second-order turbulence models for geophysical boundary layers. A review of recent work, *Cont. Shelf Res.*, *25*, 795–827.

van Beusekom, J. E. E., and V. de Jonge (2012), Dissolved organic phosphorus: An indicator of organic matter turnover?, *Estuarine Coastal Shelf Sci.*, *108*, 29–36.

Wang, Z., P. Hoekstra, H. Burchard, H. Ridderinkhof, H. Swart, and M. Stive (2012), Morphodynamics of the Wadden Sea and its barrier island system, *Ocean Coastal Manage.*, *68*, 39–57.

Zimmerman, J. T. F. (1976), Mixing and flushing of tidal embayments in the western Dutch Wadden Sea. Part I: Distribution of salinity and calculation of mixing times scales, *Neth. J. Sea Res.*, *10*, 149–191.